OFFICE OF NAVAL RESEARCH

CONTRACT N00014-84-k-0656/P00002

R & T Code 4133034

Technical Report #33

Potential Dependent Structural Changes of Underpotentially Deposited Copper on an Iodine Treated Platinum Surface Determined *In Situ* by Surface EXAFS and Its Polarization Dependence

G.M. Bommarito, D. Acevedo, J.F. Rodríguez and H.D. Abruña
Department of Chemistry
Baker Laboratory
Cornell University
Ithaca, New York 14853-1301

Prepared for Publication in
Journal of Physical Chemistry
August 25, 1993

UNCLASSIFIED

SECURITY CLASSIFICATION OF THIS PAGE

REPORT DOCUMENTATION PAGE

1a REPORT SECURITY CLASSIFICATION: unclassified	1b RESTRICTIVE MARKINGS:
2a SECURITY CLASSIFICATION AUTHORITY: unclassified	3 DISTRIBUTION/AVAILABILITY OF REPORT: unlimited
2b DECLASSIFICATION/DOWNGRADING SCHEDULE:	
4 PERFORMING ORGANIZATION REPORT NUMBER(S): Technical report # 33	5 MONITORING ORGANIZATION REPORT NUMBER(S):
6a NAME OF PERFORMING ORGANIZATION: Hector D. Abruna, Cornell University / 6b OFFICE SYMBOL (If applicable):	7a NAME OF MONITORING ORGANIZATION: Office of Naval Research
6c ADDRESS (City, State, and ZIP Code): Department of Chemistry, Baker Laboratory, Cornell University, Ithaca, New York 14853	7b ADDRESS (City, State, and ZIP Code): Chemistry Division, 800 N. Quincy St., Arlington, VA 22217
8a NAME OF FUNDING/SPONSORING ORGANIZATION: Office of Naval Research / 8b. OFFICE SYMBOL (If applicable):	9 PROCUREMENT INSTRUMENT IDENTIFICATION NUMBER: N00014-84-K-0656/P00002
8c ADDRESS (City, State, and ZIP Code): Chemistry Division, 800 N. Quincy St., Arlington, VA 22217	10 SOURCE OF FUNDING NUMBERS: PROGRAM ELEMENT NO / PROJECT NO / TASK NO / WORK UNIT ACCESSION NO

11 TITLE (Include Security Classification)
Potential Dependent Structural Changes of Underpotentially Deposited Copper on an Iodine Treated Platinum Surface Determined In Situ by Surface EXAFS and Its Polarization Dependence

12 PERSONAL AUTHOR(S)
G.M. Bommarito, D. Acevedo, J.F. Rodriguez and H.D. Abruna

13a TYPE OF REPORT	13b. TIME COVERED	14 DATE OF REPORT (Year, Month, Day)	15 PAGE COUNT
Technical	FROM _____ TO _____	1993, 08, 25	2

16 SUPPLEMENTARY NOTATION

17 COSATI CODES			18. SUBJECT TERMS (Continue on reverse if necessary and identify by block number)
FIELD	GROUP	SUB-GROUP	

19 ABSTRACT (Continue on reverse if necessary and identify by block number)

An in situ structural investigation of the underpotential deposition of copper on an iodine covered platinum surface (Pt/C layered synthetic microstructure (LSM) with Pt as the outermost layer) has been carried out using surface EXAFS (extended x-ray absorption fine structur and its polarization dependence. The effects of rinsing the electrode with pure supporting electrolyte have also been investigated. At an applied potential of +0.20V (corresponding to half a monolayer of electrodeposited copper) there are two in-plane Cu-Cu distances: 2.56±0.05Å and 4.21±0.05Å. This suggests a coexistence between a close-packed phase with a more open phase. It is likely that the open phase is stabilized by repulsive interactions between partially charged copper atoms, as well as by the presence of the strongly adsorbed iodine layer. At +0.10V (corresponding to a full monolayer of electrodeposited copper) the is only one Cu-Cu distance of 2.56±0.05Å. Combining in-plane (polarization) and out-of-plane (polarization) SEXAFS measurements, we found that at full monolayer coverage, the copper UPD layer is incommensurate with respect to the platinum surface. The iodine ad-layer rides the electrodeposited copper forming a 3x3 unit cell.

20 DISTRIBUTION/AVAILABILITY OF ABSTRACT	21 ABSTRACT SECURITY CLASSIFICATION	
☒ UNCLASSIFIED/UNLIMITED ☐ SAME AS RPT ☐ DTIC USERS	unclassified	
22a NAME OF RESPONSIBLE INDIVIDUAL: H. D. Abruna	22b TELEPHONE (Include Area Code): (607) 255-4720	22c OFFICE SYMBOL:

DD FORM 1473, 84 MAR — 83 APR edition may be used until exhausted. All other editions are obsolete.

SECURITY CLASSIFICATION OF THIS PAGE
Unclassified

Potential Dependent Structural Changes of Underpotentially Deposited Copper on an Iodine Treated Platinum Surface Determined *In Situ* by Surface EXAFS and Its Polarization Dependence

G. M. Bommarito, D. Acevedo, J. F. Rodríguez and H. D. Abruña*
Department of Chemistry
Baker Laboratory
Cornell University
Ithaca, New York 14853-1301

Abstract

An *in situ* structural investigation of the underpotential deposition of copper on an iodine covered platinum surface (Pt/C layered synthetic microstructure (LSM) with Pt as the outermost layer) has been carried out using surface EXAFS (extended x-ray absorption fine structure) and its polarization dependence. The effects of rinsing the electrode with pure supporting electrolyte have also been investigated. At an applied potential of +0.20 V (corresponding to half a monolayer of electrodeposited copper) there are two in-plane Cu-Cu distances: 2.56±0.05Å and 4.21±0.05Å. This suggests a coexistence between a close-packed phase with a more open phase. It is likely that the open phase is stabilized by repulsive interactions between partially charged copper atoms as well as by the presence of the strongly adsorbed iodine layer. At +0.10V (corresponding to a full monolayer of electrodeposited copper) there is only one Cu-Cu

distance of 2.56±0.05Å. Combining in-plane (σ polarization) and out-of-plane (π polarization) SEXAFS measurements, we found that at full monolayer coverage, the copper UPD layer is incommensurate with respect to the platinum surface. The iodine ad-layer rides the electrodeposited copper forming a 3x3 unit cell. This interfacial structure is not altered upon rinsing with pure supporting electrolyte.

Introduction

The process of underpotential deposition (UPD) [1] of metals has been extensively studied during the past two decades due to its theoretical and practical importance in fields such as electrocrystallization, catalysis, and surface chemistry. In this process, submonolayer to monolayer(s) amounts of a metal can be electrodeposited on a foreign metal substrate in a quantifiable and reproducible fashion prior to bulk deposition. Numerous electrochemical and spectroscopic techniques have been utilized to probe the mechanism(s) of formation, and the structural properties of UPD layers. Conventional electrochemical methods have been used to obtain thermodynamic and kinetic information about the UPD process [1-3]. Structural features of the UPD layer were first derived, indirectly, from equilibrium-coverage potential isotherms using single crystal substrates [3]. Non-monotonic current transients have been observed in a number of cases, and these have been interpreted in terms of mechanisms involving nucleation and growth processes. Although electrochemical methods are invaluable in controlling and measuring thermodynamic parameters such as applied potential, charge, and coverage, structural inferences are indirect and often model dependent.

Surface sensitive ultra high vacuum techniques have been employed in the study of UPD systems and much information has been obtained from them [4]. However, the fact that these studies are inherently *ex situ* raises some fundamental questions as to their applicability.

Hubbard *et al.* employed electron spectroscopic techniques to obtain direct atomic structural information about metal deposits on an iodine covered Pt(111) surface [5]. They found that electrodeposition occurred in a well-defined manner, with the formation of different structures depending on the coverage. Although these *ex situ* experiments provided a wealth of information, it is unclear what structural changes may have occurred to the UPD layer upon transfer of the electrode from solution to vacuum. In addition, these experiments do not provide structural information about the solution side of the double layer, an integral part of the system at equilibrium with the adsorbed species.

The use of atomic resolution microscopic techniques has provided the means to obtain *in situ* direct atomic structural information on UPD systems. Scanning tunneling and atomic force microscopy have been recently employed in the study of UPD processes including copper UPD on gold and platinum surfaces [6]. These studies have shown that the UPD process occurs in a well-defined manner and that the structures observed from these experiments are similar to those observed in vacuum. As was the case in the *ex situ* experiments, these techniques provide information only for the deposited layer.

Recently, *in situ* x-ray spectroscopic and diffraction techniques have provided unique atomic resolution structural information about UPD systems [7]. Extended x-ray absorption fine structure (EXAFS) and x-ray absorption near edge structure (XANES) have been employed in the study of various UPD systems [8], providing information about the local structure, atomic environment and the

oxidation state of the adsorbed species. Specific systems that have been studied include Cu on Au(111) and Au(100), Ag on Au(111), Pb on Ag(111), Tl on Ag(111) and others [8].

Furthermore, surface x-ray scattering measurements have been used to study the in-plane structure of some UPD systems [9].

In addition to these techniques, x-ray standing waves (XSW) have been utilized to probe the electrochemical double layer [10,11]. In these studies, one can obtain information pertaining to the distribution of species, including the diffuse layer, in a direction normal to the substrate's surface.

In this paper, we present the results of a series of *in situ*, polarization dependent surface EXAFS experiments aimed at probing the potential dependent structure of underpotentially deposited copper on an iodine covered platinum/carbon layered synthetic microstructure and discuss our findings within the framework of surface structures, their coverage dependence and the influence of the iodine ad-lattice.

Theoretical description

EXAFS refers to the modulations in the x-ray absorption coefficient beyond an absorption edge [12]. Such modulations can extend up to about 1000 eV beyond the edge and generally have a magnitude of less than 15% of the edge jump. The frequency of the EXAFS oscillations depends on the distance between the absorber and its near neighbors, whereas the amplitude depends on the numbers and types of neighbors as well as their distance from the absorber. From an analysis of the EXAFS one can obtain information on near

neighbor distances (to ±0.01Å), numbers (to ±15%) and types (assuming a significant difference in atomic number).

The EXAFS represents the normalized modulation of the absorption coefficient as a function of energy. In wave vector form the EXAFS can be expressed as a summation over the various coordination (near neighbor) shells and is given by:

$$\chi(k) = \sum_j \frac{1}{kr_j^2} N_j F_j(k) S_i(k) \exp^{-\sigma_j^2 k^2} \exp^{-2r_j/\lambda(k)} \sin(2kr_j + \phi_j(k)) \qquad (1)$$

where k represents the wave vector, r_j is the absorber-backscatterer distance and N_j is the number of scatterers of type j with backscattering amplitude $F_j(k)$. The product of these last two terms gives the maximum amplitude. There are also amplitude reduction factors. $S_i(k)$ takes into account many-body effects such as electron shake-up and shake-off processes, whereas the term $\exp^{-\sigma j^2 k^2}$ (known as the Debye-Waller factor) accounts for thermal vibration and static disorder. Finally, the term $\exp^{-2kj/\lambda(k)}$ takes into account inelastic scattering effects where $\lambda(k)$ is the mean free path of the photoelectron.

The oscillatory part of the EXAFS: $(\sin(2krj + \phi j(k))$, takes into account the relative phases between the outgoing and backscattered waves. Since the accuracy of the determination of interatomic distances depends largely on the appropriate determination of the relative phases, a great deal of attention has been given to this aspect. This can be achieved by ab-initio calculation of the phases involved [13] or alternatively they can be determined

experimentally through the use of model compounds and the concept of phase transferability [14]. We have carefully considered the differences between phase shifts calculated ab-initio and phase shifts determined from measurements of reference materials (Figure 1). Referring to Figure 1, we note that there is excellent agreement between the phase shifts measured from reference materials and the calculated values [13] for absorber-scatterer pairs likely to be important in this study (i.e. Cu-Cu, Cu-Pt, and Cu-I). This agreement extends over the k-space range from 3 to 10 $Å^{-1}$, with the largest discrepancy between calculated and measured phase shifts amounting to ±10%. As a consequence of this favorable comparison, we decided to use phase shifts determined from reference materials.

SEXAFS [15] differs from conventional EXAFS of polycrystalline or amorphous materials in that the polarization of the incident x-ray beam strongly influences the amplitude of the EXAFS oscillations so that bonds whose vector lies in the plane of polarization contribute significantly to the observed oscillations whereas bonds whose vector is normal to the polarization plane will not. For SEXAFS of K edges, the effective coordination number for a particular shell, N_{eff}, is approximately related to the true coordination number N by:

$$N_{eff} = 3 \sum_{i=1}^{N} \cos^2 \theta_i \qquad (2)$$

where θ_i is the angle between the vector connecting the absorber and its neighbor and the electric field vector (E-vector) of the incident beam [16]. Thus, as mentioned above, if the polarization of the incident beam is perpendicular to the surface, the absorber's

neighbors which lie parallel to the surface will not contribute to the EXAFS signal and vice-versa. This selection rule is frequently employed in SEXAFS studies in order to determine bonding geometries.

Experimental

The experiments were carried out at the Cornell High Energy Synchrotron Source (CHESS), under parasitic conditions (5GeV, 60-100 mA), using the B-2 beam line. White beam radiation enters the experimental hutch through a thin beryllium window and passes through a double-crystal Si(111) monochromator. The monochromator resolution was approximately 1.0 eV at 9.0 keV. The emerging beam is collimated by vertical and horizontal slits. The beam incident onto the sample had a height and width of 0.04 and 4 mm, respectively. A high degree of collimation is needed because of the geometrical constraints imposed by the grazing incidence geometry, and to ensure that, to a good approximation, the incident beam is a plane wave. Ion chambers were used to measure the incident and reflected intensities, while a Si(Li) solid-state detector was used in conjunction with a spectroscopy amplifier, and a single channel analyzer to measure the Cu Kα fluorescence. The detector resolution was 150 eV at 6.0 keV. The incident energy was scanned over the range of 8.8 to 9.7 keV. The incident flux was approximately 10^9 photons/s.

The electrochemical cell, housed inside an aluminum holder, consisted of a cylindrical Teflon body with feedthroughs for electrolytes and electrode connections. The cell was thoroughly

cleaned prior to use. This cleaning procedure involved an initial overnight wash in No-chromix and concentrated H_2SO_4, followed by a 30 minute wash in hot concentrated 1:1 HNO_3/H_2SO_4 solution, and a thorough rinse in pyrolitically distilled water (PDW) [17]. The filling and rinsing of the cell with electrolyte was accomplished with pressurized glass vessels through the fluid feedthroughs. A thin layer of solution (approx. 2-5 μm thick) was trapped between the electrode, and a 6.35 μm thick polypropylene film which was held in place by a Teflon ring. All the electrochemical measurements were conducted with the polypropylene film distended by the addition of excess bulk electrolyte into the cell. The thin layer was then restored by removing excess electrolyte. Potential control of the electrode was retained through filling and rinsing stages. All potentials are reported with respect to a Ag/AgCl (1M NaCl) reference electrode.

Electrochemical experiments were carried out with a Princeton Applied Research model 173 potentiostat in conjunction with a model 175 universal programmer and 179 digital coulometer. Voltammograms were recorded on a Soltec X-Y recorder.

Platinum/carbon LSMs of dimensions 15 mm by 20 mm were obtained from Ovonic Synthetic Materials Co. (Troy, MI). The LSMs used had d-spacings of 39.7 Å or 41.4 Å, and consisted of 200 layer pairs of platinum and carbon with platinum as the outermost layer, deposited on a 0.015 in. thick Si(111) substrate.

The electrolyte was 0.10 M sulfuric acid (Baker Ultrex) containing 0.50 mM copper sulfate (Aldrich Gold Label) and was prepared using pyrolytically distilled water [17]. The Pt/C LSM was

cleaned by a series of oxidation-reduction cycles (at 20mV/sec) in pure supporting electrolyte (0.1M sulfuric acid) followed by formation of the iodine ad-layer which was formed by contacting the electrode with a 1mM solution of NaI in 0.1M sulfuric acid for 15 min. Afterwards, the electrode was rinsed with supporting electrolyte. Prior to copper deposition, electrolyte solution was added to the cell so that the polypropylene film distended somewhat, thus allowing the UPD layer to be deposited from bulk electrolyte. The monolayer was deposited from bulk electrolyte because of the low copper concentration. Deposition was carried out at constant potential for 15 min. after which the current had decayed to background levels. Deposition potentials of +0.20V and +0.10V vs Ag/AgCl corresponding to copper coverages of one-half and a full monolayer, respectively were employed in the SEXAFS studies. After deposition, part of the electrolyte solution was withdrawn, leaving only a thin layer of electrolyte, whose thickness was determined from reflectivity measurements. The amount of copper ions contained within the thin layer typically represented about 2-5% of the amount electrodeposited on the surface. As a result, no interference from copper in solution was anticipated.

All experiments were performed at room temperature. Data were collected in scans of about 20 minutes and approximately 40-50 scans were averaged. Data were analyzed using standard procedures which involved background subtraction employing polynomial splines and conversion to wavevector. Data were typically multiplied by k to weight more evenly the contribution at larger k values relative to lower k values. A FFT routine was used to

obtain a modified radial distribution function. Fourier windows were employed to isolate a particular shell and the data were transformed back to k space where all fittings for phase and amplitude were done using non-linear least squares analysis. Data over the range of 3-10$Å^{-1}$ were typically considered. At lower k values one needs to take into account contributions from multiple scattering and at larger values the amplitudes of the modulations have essentially decayed. Bond distances were obtained by fitting the oscillatory part of the EXAFS expression to the experimental oscillations with phase shifts obtained from reference materials which included copper foil, CuO, CuI and $CuPt_3$.

Results and Discussion

A. Electrochemistry

In these experiments, a platinum/carbon layered synthetic multilayer (LSM) with platinum as the top-most surface was used as the working electrode. This type of substrate was chosen since the LSM could also serve as a Bragg diffracting structure for x-ray standing wave (XSW) measurements. The results of these XSW experiments will be reported elsewhere [18].

Although indirectly, electrochemical measurements can yield structural information regarding the LSM's platinum surface by comparison to electrochemical experiments with electrode surfaces that are structurally well-defined. For example, in sulfuric acid media, the voltammetry due to the platinum surface of the LSM showed only one pronounced (weakly bound) hydrogen adsorption

peak (Figure 2A). Such behavior has been previously shown to be characteristic of a clean, well-ordered (i.e. atomically smooth over large coherence lengths) Pt(111) electrode which has been subjected to a few cycles in which a surface oxide is formed and then removed (Figure 2B). This cycling results in a Pt(111) surface with nearly randomly distributed mono-atomic steps [19].

We chose to study the underpotential deposition of copper on an iodine covered platinum surface in part because the iodine ad-layer renders the surface chemically impervious to contamination [5]. In addition, XSW experiments on the electrosorption of iodide/iodine on a platinum/carbon LSM have shown that the iodine ad-layer appears to undergo similar potential dependent structural re-arrangements on LSMs [11a] as on Pt(111) single crystal electrodes [20,21]. The UPD of copper on such a surface has been shown to displace the iodine ad-layer, and deposit directly onto the platinum surface [5,22].

Figure 3A shows the cyclic voltammogram for copper deposition (in 0.1M sulfuric acid containing 0.5 mM $CuSO_4$) on an iodine covered (adsorption from a 1mM NaI aqueous solution) platinum/carbon LSM used as the working electrode. Although the anodic and cathodic branches have different shapes, the charge under them is equivalent. By holding the potential at values between +0.40 and +0.10 V (vs. Ag/AgCl reference) the surface coverage of copper can be systematically controlled to vary from essentially zero up to a monolayer. Referring to Figure 3A, we observe only one pronounced deposition wave at a peak potential value of +0.20 V and a half-width of approximately 40 mV. A

shoulder is also visible at +0.12V before the onset of bulk deposition at 0.0V. The charge under this deposition wave was on average $487 \pm 50\ \mu C/cm^2$. The stripping wave is considerably broader (approx. 100 mV) with two resolved peaks at +0.14V and +0.25V, corresponding to a total charge of $482 \pm 50\ \mu C/cm^2$. It is also important to note that the cyclic voltammogram of copper UPD on a Pt(111) electrode that has been oxidized-reduced a few times, followed by the adsorption of iodine, is virtually identical (Figure 3B). This further confirms the structural similarities between these two types of surfaces.

The SEXAFS measurements were carried out at applied potentials of +0.20V and +0.10V which correspond to nominal copper surface coverages of one-half and a full monolayer, respectively. Furthermore, we conducted a series of SEXAFS measurements after "rinsing" the electrode (at least three times with clean supporting electrolyte) while holding the applied potential at +0.10V. The SEXAFS measurements were then carried out without bulk Cu^{+2} present in the supporting electrolyte.

B. Coverage Measurements

Figure 4a shows the electrochemical coverages plotted in monolayer units (ML) at deposition potentials of: +0.25V, +0.20V, +0.15V, and +0.10V, determined by integrating the charge under the anodic current peaks in the corresponding cyclic voltammograms. In these measurements it is assumed that the electrochemically active area of the electrode surface is accurately determined by measuring

the charge due to hydrogen adsorption in the cyclic voltammogram of Figure 2.

Figure 4a represents coverage isotherms obtained for both no rinsing and rinsing experiments as defined previously. In the no rinsing measurements, where the UPD copper layer was stripped from the surface in the presence of bulk copper species, the charge under the deposition and stripping peaks for various surface coverages was equal. In the rinsing experiments, where the deposited layer is stripped after rinsing with pure supporting electrolyte (hence in the absence of bulk Cu^{+2} species), we observe large differences between the deposition and stripping charges. This difference indicates the loss of substantial fractions of the deposit upon rinsing. Furthermore, the amount of deposited copper lost due to rinsing is coverage dependent. Referring to Figure 4a, at full monolayer we observe a loss in coverage upon rinsing of only 16%. In contrast, for initial coverages of 3/4, 1/2, and 1/4 of a monolayer there are dramatic losses of 47%, 55%, and 62%, respectively. This behavior is rather surprising since, in principle, the UPD layer is in equilibrium with the copper ions in solution, and removal of this bulk component should result in complete desorption of the electrodeposited monolayer. In comparison, at a bare (i.e. no iodine ad-layer) platinum surface of a platinum/carbon LSM, rinsing at any initial coverage results in the complete desorption of the UPD layer. Hence, it appears that the presence of an initial ad-layer of iodine "stabilizes" the UPD layer against desorption induced by the loss of copper ions in the bulk solution phase. This stabilization is considerably stronger for a fully formed UPD layer as opposed to a

partial deposit, suggesting some stabilization due to copper-copper interactions.

The coverage isotherms determined from x-ray fluorescence measurements are displayed, using a normalized scale, in Figure 4b. This figure shows two sets of data, representing a similar series of no rinsing and rinsing experiments as the ones described above. Although we observe a loss of coverage upon rinsing, the fractional losses found in these x-ray measurements are considerably larger than those measured electrochemically (Figure 4c). In order to make a quantitative comparison of the isotherm derived from both x-ray and electrochemical measurements, data were normalized at one point: +0.1V after rinsing and the results are presented in Figure 5. Based on these results we draw the following conclusions:

(1) For the rinsing experiments the isotherms derived from electrochemical and x-ray measurements are in excellent agreement.

(2) Comparison of the no rinsing isotherms points out the presence of a considerable amount of copper, which appears to be electrochemically inactive.

(3) The amount of this electrochemically inactive copper is potential dependent, and well above the amount of bulk copper (in the form of Cu^{+2} ions) present in solution. XSW measurements carried out concurrently with these SEXAFS experiments, place this excess copper at the electrode/electrolyte interface [18].

(4) Even for applied potentials of +0.45V, where no electrodeposition occurs, we observe an amount of copper equivalent to approximately 20% of a monolayer.

(5) The iodine coverage, as determined by x-ray fluorescence measurements, remains constant throughout the experiments.

C. XANES

We begin the discussion of the SEXAFS experiments by presenting the x-ray absorption near edge structure (XANES) for underpotential deposition at +0.1V without rinsing (Figure 6). For comparison, we also show in Figure 6 the XANES of some reference materials. Features in the XANES spectra are typically quite sensitive to the structure and chemical nature around the absorbing atom (copper in the present case). XANES measurements are also very valuable in identifying the oxidation state of the absorbing atom. Quantitative interpretation of these data however is difficult since it requires use of a complicated multiple-scattering formalism. However, from a qualitative standpoint a number of useful conclusions can be drawn. Firstly, the energetic location of the edge is dependent on the oxidation state of the absorbing atom. Referring to Figure 6, we observe the edge rise for the UPD monolayer to be at an energy of 8.981 keV, coincident with the edge rise in a copper metal foil and the $CuPt_3$ alloy. This is to be contrasted with the spectra for CuI, CuO, and $CuSO_4$. The edge position in the CuI reference is approximately 5 eV more positive, whereas for the CuO and $CuSO_4$ references the edge is shifted even further, to values of 8.987 and 8.990 keV, respectively. Furthermore, the edge feature approximately half-way up the edge jump in the UPD spectra is also observed in the copper metal foil as well as the $CuPt_3$ alloy references. This feature is often taken to be the signature for the

presence of metallic copper. The characteristic "white-line" feature observed at the edge for the CuI, CuO, and $CuSO_4$ references is not observed in the electrodeposited copper spectrum. The absence of such a feature is further indication that the electrodeposited copper appears to be fully discharged.

Next we compare the first few oscillations observed immediately beyond the edge which are quite sensitive to the structure and chemical nature of the species around the copper center. Of particular importance are the differences in the relative intensities and frequency of the oscillations. The CuO and $CuSO_4$ spectra (Figure 6) are essentially featureless beyond the prominent white-line. In the CuI reference, the white-line feature is followed by a weak peak at 8.998 keV and a more prominent one at 9.016 keV. The copper metal foil reference shows three clearly resolved peaks at 8.998 keV, 9.008 keV, and 9.030 keV. Finally, the $CuPt_3$ alloy spectrum displays a peak at 8.997 keV with a visible shoulder, followed by a second peak at 9.020 keV. In the copper UPD XANES data we also observe a first peak at 8.997 keV with a shoulder, and a second more symmetric peak at 9.022 keV. The separation between these two features is 25 eV, which coincides almost exactly with the separation between the two peaks observed in the $CuPt_3$ alloy. It appears that the structure around the electrodeposited Cu at full coverage, is very similar to that of the $CuPt_3$ alloy in contrast to that of CuI or copper metal foil references. This suggests that the structure around the copper center in the UPD monolayer is significantly influenced by the presence of the platinum substrate. This is consistent with the observation that upon underpotential

deposition, copper atoms displace the iodine ad-layer and deposit directly onto the platinum surface of the LSM.

Finally, it is important to compare the potential dependence of the near edge features. This is done in Figure 7, where we plot the XANES for UPD layers deposited at +0.1V, +0.2V, +0.25V, and +0.45V without rinsing. These potentials correspond to nominal coverages of full, 1/2, 1/4, and no coverage, respectively. In addition, we also show the XANES for deposition at +0.1V, followed by rinsing with pure supporting electrolyte. The first thing to note is that the intensity offsets in this figure are meaningful, and represent changes in coverage. These changes are in excellent agreement with the results presented in the discussion of electrochemical and x-ray determined coverages for no-rinsing experiments. When we compare the intensity offset for deposition at +0.1V before and after rinsing we observe a loss of coverage of approximately 20%. This agrees well with the loss of coverage measured electrochemically (Figure 4a). In contrast, it is considerably smaller than the loss determined from x-ray fluorescence measurements (Figure 4b). To explain this observation one must consider that the XANES measurements shown here are carried out at an angle of incidence, θ, just slightly below the critical angle θ_c of the platinum/carbon LSM. Under this condition ($\theta \approx \theta_c$) the electric field of the standing wave formed by the superposition of the incident and totally externally reflected x-ray waves has an antinode right at the surface [10]. An exponentially decaying evanescent wave with a small penetration depth (20-30 Å) extends below the surface. The net effect of this scattering geometry is to maximize the fluorescence signal from the

deposited layer right at the electrode/electrolyte interface, while minimizing the contribution from the bulk material in solution or from copper ions distributed in a diffuse layer extending out some distance from the electrode. Hence, it is reasonable that the difference in coverage between rinsing and no rinsing experiments reflected in these XANES measurements is closer to that determined electrochemically. Because coverages determined through x-ray fluorescence measurements were performed at an angle of incidence much larger than θ_c (and smaller than the Bragg angle θ_B for the Pt/C LSM), they would reflect the existence of a diffuse layer of copper ions in addition to the UPD layer. Furthermore, under this geometry ($\theta_c<\theta<\theta_B$) the intensity of the reflected x-ray wave is extremely small (10^{-8}), and as a result there is no surface enhancement effect due to the presence of a standing wave field as described above.

The intensity and frequency of the oscillations beyond the edge do not appear to be potential dependent. All spectra in Figure 7 are quite similar to that of the $CuPt_3$ alloy. We do note however, a slight shift toward higher energies in the location of the edge as a function of decreasing coverage (increasing potential). Furthermore, the feature observed half-way up the edge becomes somewhat less prominent as the coverage decreases. These two observations seem to imply a "charging" of the UPD species as a function of increasing potential or decreasing coverage. More realistically, we would conclude that it is possible that at submonolayer coverages charge transfer upon deposition is not complete so that the copper species are not fully discharged.

What is important to note, however, is the large positive shift (ca. 9 eV) in the edge position as well as the appearance of a white-line feature when the applied potential is +0.45V. Recalling that no deposition occurs at this potential, the XANES spectrum under these conditions is due to the bulk Cu^{+2} ions only. Furthermore, the only way we could measure this signal was to fully extend the thin layer of the electrochemical cell, allowing for an additional increase in the volume of bulk solution of approximately 20 times the normal amount. No detectable signal could be measured under the normal thin layer condition, at this potential. This is a very important observation for two reasons:

(1) It demonstrates we can reversibly deposit and completely strip the UPD layer.

(2) It points out that the bulk contribution to the UPD SEXAFS signal is negligible at a bulk $CuSO_4$ concentration of 0.5 mM.

D. SEXAFS

In this section we discuss the results from polarization dependent SEXAFS measurements of:

(1) Copper underpotential deposition at +0.10V (nominal full coverage), before and after rinsing.

(2) Copper deposition at +0.20V (half-monolayer coverage) without rinsing.

We begin by discussing the case of deposition at +0.10V after rinsing with supporting electrolyte. As we have previously mentioned, rinsing the electrode results in a loss of coverage amounting to approximately 20%, from 0.85 ML to 0.68 ML. These

absolute values of coverage were determined electrochemically by measuring the charge under the anodic stripping wave. Figure 8 shows the SEXAFS spectra for deposition at +0.10V after rinsing, and with the plane of polarization of the incident x-ray beam being either parallel (σ polarization) or perpendicular (π polarization) to the electrode surface. The polarization orientation in these experiments is of fundamental importance. σ polarized SEXAFS measurements are sensitive only to in-plane bonds; that is bonds having a non-zero projection in the plane of the electrode surface. On the other hand, π polarized SEXAFS measurements can only measure the component of a given bond normal to the electrode surface. The data shown in Figure 8 represent the average of approximately 40 to 50 individual scans, with each scan taking approximately 20 to 30 minutes to acquire. Although not easily discerned in these raw data, there are some differences in the relative intensity and frequencies of the SEXAFS oscillations. These data were analyzed using the methodology described in the experimental section.

The resulting radial distributions are shown in Figures 9A and 10A. Considering the k-weighted radial distribution for the σ polarization case first (Figure 9A), we observe two prominent but unresolved peaks at 1.01 Å, and 2.16 Å. It should be noted that the data in these radial distribution functions are not phase corrected and thus the distances are shorter than the actual values which we will present in a later table. There are two ways in which we can interpret unresolved peaks in a radial distribution function:

(1) There are several chemically distinct backscattering species within a given coordination shell.

(2) There are two chemically identical shells which are not resolved.

Given these two possible interpretations, data analysis of this radial distribution was conducted as follows:

(1) Each of the two prominent peaks was individually filtered and back-transformed to reciprocal space or k-space, resulting in two distinct data sets.

(2) The back-transformed data from 3 to 10 $Å^{-1}$ was fitted for phase and amplitude trying both: single backscatterers models (i.e. I only, Cu only, and Pt only), or two backscatterers models (i.e. I and Pt, Pt and Cu, and I and Cu). It is important to consider what parameters were varied in our model to fit the data (refer to Equation 1). Once the backscatterer(s) is determined, hence determining the phase shift $\phi_j(k)$, in order to fit the phase or oscillatory portion of each back-transformed data set only one fitting parameter, r_j or the bond length between the electrodeposited copper center and its backscatterer, was varied. To fit the amplitudes of the back-transformed data, the fitting parameters varied in our model were: N_{eff}, the effective number of nearest neighbors, σ_j, the Debye-Waller factor which takes into account static disorder and thermal vibrations, and a normalization constant. $F_j(k)$ was determined using fits to data collected from reference materials, once a particular backscatterer had been chosen. The best fit for each of the two data sets was then accepted. We found that to best fit the peak at 1.01 Å a model including both I and Pt backscatterers was necessary. For the second peak in the radial distribution of

Figure 9A (2.16 Å), the best fit was obtained using a model with only Cu as a backscatterer.

(3) Both peaks in the radial distribution were then filtered (filter window is shown for this case as a dashed line on Figure 9A), and back-transformed into k-space (Figure 9B, filled circles).

(4) Using the fitting parameters determined in step (2) above as initial values, the back-transformed data from (3) was fitted once again for phase and amplitude using a model which included all three backscatterers (I, Pt, and Cu). This step had the effect of refining the parameters, and never altered the initial values extracted from step (2) by more than 10 to 20%. The fit from this final step is shown as a dashed line in Figure 9B, and the final values of the fitting parameters are presented in Table I.

As mentioned above, we have found that the 1.01 Å peak in the radial distribution of Figure 9A originates from both Cu-I and Cu-Pt interactions, whereas the peak at 2.16 Å is due to Cu-Cu interactions. Referring to Table I, we report the in-plane projection of the Cu-Cu bond length to be 2.54±0.05 Å. This value is virtually identical (within error bars) to the atomic Cu-Cu bond length (2.56 Å), implying that the Cu UPD layer is close-packed. This is consistent with the conclusion drawn from XANES data that the electrodeposited copper is metallic, since repulsive interactions between partially charged copper species would tend to produce a considerably more open lattice. The effective number of copper nearest neighbors was found to be 6.4±1.5 also in good agreement with an hexagonal close-packed UPD layer.

The in-plane projections of the Cu-Pt and Cu-I bond lengths were found to be 1.41±0.05 Å and 1.52±0.05 Å, respectively. To gain some insight into the significance of these bond lengths, we can compare them to the in-plane projected bond lengths expected from model structures. We begin by considering the Cu-Pt bond. If we assume the surface of the LSM to be a randomly stepped (111) oriented surface (vide-supra), then there are three likely sites for deposition: a three-fold hollow site, a bridge site, and a top site. A Cu-Pt top site bond will have no in-plane projection, and in the σ polarized SEXAFS measurement we should have not observed Pt backscattering. The fact that in order to fit the data Pt backscatterers were necessary, in addition to the qualitative but striking similarities of the UPD XANES data to that for the $CuPt_3$ alloy reference, rules out the presence of top site Cu-Pt bonds. If all electrodeposited copper atoms were to sit in three-fold hollow sites, thus forming an epitaxial overlayer, the in-plane projected bond length would be 1.61 Å. Deposition at bridge sites only, would result in an in-plane projected bond length of 1.39 Å. The experimental value of 1.41±0.05 Å measured here is in good agreement with the bridge site position. However, since we have already determined that the copper UPD layer is hexagonal close-packed, and given that the Pt-Pt bond length for the (111) surface is 2.78 Å, we conclude that the copper monolayer is incommensurate, over small length scales, with respect to a Pt(111) orientation. Hence, although we would anticipate a range of positions to be occupied (Figure 11) including top, three-fold hollow, and bridge sites, the resulting Cu-Pt bond length averages out to a value close to that corresponding to a

bridge site. The spread about this average value must be relatively narrow, since a large spread would likely dampen the contributions of this absorber-backscatterer pair to the SEXAFS. Thus, we speculate that although incommensurate over short length scales, the copper UPD overlayer is in registry with the underlying platinum surface if we were to consider a large unit cell. However, without specific knowledge of the orientation of the incommensurate UPD layer with respect to the underlying substrate, it is difficult to verify that this interpretation is indeed correct. The effective number of platinum nearest neighbors (see Equation 2) was found to be 0.6±0.2. This is in closer agreement (within error bars) to the N_{eff} value expected from a model bridge site (0.54) rather than a three-fold hollow site (1.08).

Considering a close-packed copper UPD layer with a Cu-Cu bond length of 2.54±0.05 Å, we can identify once again three likely sites for adsorption of an iodine atom. The expected in-plane projected Cu-I bond lengths for such a model are: 1.48 Å, 1.28 Å, and 0 Å for three-fold hollow, bridge, and top sites, respectively. The measured value of the in-plane projected Cu-I bond length is 1.52±0.05 Å, which is in good agreement with a three-fold hollow site on this close-packed copper overlayer. Furthermore, N_{eff} is found to be 1.2±0.5 which is in good agreement with the value expected for a three-fold hollow site (1.6), in contrast to that for a bridge site (0.8).

To summarize, the σ polarized SEXAFS data discussed above is consistent with a model in which the copper UPD layer is close-packed, with a Cu-Cu bond length equivalent to that of bulk copper, and incommensurate, over a short length scales, with respect to a

platinum surface with a (111) orientation. The iodine appears to adsorb at three-fold hollow sites on the copper UPD layer, consistent with the formation of an epitaxial ad-layer.

In order to triangulate and confirm this structure we also carried out a complete set of SEXAFS measurements for deposition at +0.10V after rinsing, using π polarization. Figure 10A shows the k-weighted radial distribution resulting from analysis of the raw SEXAFS data in Figure 8. In this distribution we observe two unresolved peaks at 1.88 Å and 2.74 Å (once again, recall that these data are not phase corrected). These data were analyzed following the series of steps outlined previously. The best fit resulting from this procedure is shown as the dashed line in Figure 10B. The final fitting parameters are shown in Table I. Referring to this table, we assign the lower peak at 1.88 Å in the radial distribution of Figure 10A to Cu-Pt backscattering. Note that the data was best fit by using a model which did not involve Cu-Cu backscattering. This implies that the UPD layer lies within a single plane rather than in a bilayer or multilayer arrangement. The lack of copper backscatterers also eliminates the possibility that the copper deposits in three-dimensional clusters. The out-of-plane projected Cu-Pt bond length was determined to be 2.44±0.05 Å. Once again, assuming the platinum surface orientation to be (111) like, we would expect out-of-plane projected bond lengths of 2.13 Å, 2.28 Å, and 2.67 Å for a three-fold hollow, bridge, and top sites, respectively. The observed value of 2.44±0.05 Å lies between the values characteristic of a bridge and top site. Arguing once again that the copper UPD layer is incommensurate with respect to the platinum surface lattice, we

would expect a range of sites to be occupied, with an average value for the Cu-Pt distance of 2.44±0.05 Å. As before, without specific knowledge of the orientation of the UPD layer with respect to the surface we cannot verify this claim.

The out-of-plane projected Cu-I bond length was found to be 3.10±0.05 Å. If we consider the bond lengths calculated for adsorption sites on a close-packed copper UPD layer (Table II), the value measured here is in remarkable agreement with that for a three-fold hollow site. If we combine the σ and π polarization measurements, and triangulate the structure to determine the average Cu-Cu, Cu-I, and Cu-Pt bond lengths we obtain: 2.54±0.10 Å, 3.45±0.10 Å, and 2.82±0.10 Å respectively. These values are in excellent agreement with the expected bond lengths calculated using atomic radii for copper and platinum and the Van der Waal radius of iodine (Table II).

Based on these σ and π polarization SEXAFS measurements, we propose the model shown in Figure 11 to describe the full-coverage structure of copper, produced by underpotential deposition at +0.10V and after rinsing with pure supporting electrolyte. In this model, we will assume (based on the arguments presented before) that the platinum surface of our LSM is well represented by one that is randomly stepped (111) in character. The electrodeposited copper forms a close-packed incommensurate layer with a Cu-Cu bond length of 2.54±0.05 Å. Adsorption of iodine at the UPD layer occurs on three-fold hollow sites to form an epitaxial ad-layer with a 3x3 unit cell. It has been previously demonstrated that iodine can form a 3x3 ad-layer on a bare Pt(111) surface [23], in the potential range

from +0.10V to +0.80V vs Ag/AgCl, at a pH of 4. Here we observe an identical iodine ad-layer packing at a potential within the range specified above, but on a close-packed copper monolayer and at a pH of 1.

The full coverage structure in Figure 11 can be compared to other models proposed for similar systems. Based on an analysis of LEED and Auger data, Hubbard and co-workers estimated a Cu-Cu distance of 4.16 Å for half a monolayer of copper underpotentially deposited on an iodine treated Pt(111) single crystal [5]. Such a Cu-Cu bond length can be achieved if the electrodeposited copper atoms initially occupy a particular set of three-fold hollow and bridge sites to achieve an open 3x3 unit cell with a coverage Γ_{Cu}=4/9. At full coverage (Γ_{Cu}=8/9), Hubbard et al. propose a model in which all three-fold hollow sites are occupied, producing a commensurate but "buckled" copper overlayer with an overall Cu-Cu bond length of 2.54 Å, but with an in-plane projected Cu-Cu bond length of 2.41 Å. This distance is considerably shorter than the bulk Cu-Cu distance which is what we observe. It is possible that the difference between our model and that of Hubbard on a Pt(111) surface is due to the presence of a higher density of monoatomic steps on our platinum surface. Defects such as these could provide a series of higher coordination sites forming a template for nucleation of an incommensurate close-packed UPD structure rather than an epitaxially commensurate overlayer. One further point to note is that both Hubbard's and our model, the iodine forms a commensurate 3x3 ad-layer on the electrodeposited copper. The model proposed here can also be contrasted to the underpotential

deposition of copper on Au(111) [8], where the copper occupies three-fold hollow sites and forms a commensurate lattice. Once again, we believe the existence of steps on our "real" surface as well as the presence of an iodine ad-layer, significantly modifies the energetics of the interface favoring the formation of a close-packed incommensurate structure. Furthermore, in previous EXAFS studies on copper and silver UPD on Au(111) [8] strong scattering by oxygen, which was attributed to water and/or electrolyte ions in contact with the UPD monolayer, was observed. In the present case we saw no evidence for scattering by oxygen, which is consistent with the fact that at the potentials where these studies were carried out the iodine, which is the top-most layer, is assumed to be neutral as well as hydrophobic [23]. This would preclude co-adsorption of an oxygen containing species such as HSO_4^-. It is thus clear that such ad-layers can profoundly affect the structure and distribution of interfacial species. Similar findings have been recently reported for Cu UPD on Pt(111) in the presence of chloride anions. [24] Thus, the presence of co-adsorbed halides appears to lead to a common mechanism of deposition.

Finally, we would like to discuss SEXAFS measurements carried out as a function of deposition potential but without rinsing the electrode with supporting electrolyte. We begin by discussing deposition at +0.10V. The raw σ polarized SEXAFS spectrum is shown in Figure 12A, and the k-weighted radial distribution obtained from analysis of this data is depicted in Figure 13c. Comparing these data to those for deposition at +0.10V followed by rinsing (Figure 9A), we observe a similar sequence of unresolved peaks at 1.10 Å and 2.12

Å. Furthermore, the relative intensity of the two peaks in both radial distribution functions is essentially the same. In addition, in both radial distribution functions the peak at 2.12 Å has a weak shoulder at 2.80 Å. Fitting the back-transformed data using an identical procedure to that discussed above, yields the results listed in Table I. Once again, comparison to the results from the +0.10V rinsing experiments shows that the interfacial structure formed in these two cases is virtually identical. The clear implication is that rinsing at full coverage does not alter the structure of the UPD layer. This is consistent with our earlier conclusion that the large coverage loss observed in the x-ray fluorescence measurements upon rinsing at +0.10V, is due to the removal of copper species in a diffuse layer loosely bound at the interface, rather than the loss of a large fraction of electrodeposited copper atoms. Furthermore, it is a most important observation since it confirms the hypothesis that the presence of the iodine ad-layer can stabilize the full-coverage UPD structure even upon removal of the bulk component of the system. It also implies that underpotential deposition in the presence of a strongly adsorbed species is thermodynamically a non-equilibrium process.

At +0.20V without rinsing (Figure 12B), the k-weighted radial distribution obtained from the σ polarized SEXAFS (Figure 13b) is dramatically different from that at +0.10V. The most distinctive difference is the appearance of peaks at 4.00 Å and 4.92 Å. Comparison to a copper foil reference (Figure 13a) shows that these peaks are in virtually the same locations as the peaks corresponding to the second and third shells of the copper foil. The peak at 4.00 Å

was fitted using the Cu-Cu second shell reference. Furthermore the 1.10 Å peak in the radial distribution at +0.10V is barely distinguishable as a weaker shoulder at 1.48 Å for deposition at +0.20V. As a result, the back-transformed data corresponding to the window shown in Figure 13b can be adequately fitted using a model involving only Cu-Cu and Cu-I interactions. The results are presented in Table I. Referring to this table we find two in-plane Cu-Cu bond lengths: 2.56±0.05 Å and 4.21±0.05 Å. This implies that at a potential of +0.20V (without rinsing) the UPD layer consists of two coexisting phases: a close-packed phase similar to that observed at +0.10V, and a considerably more open phase (Figure 11B). The Cu-Cu bond length of this open phase is consistent with the 3x3 overlayer structure observed by Hubbard et al. on Pt(111) at a coverage Γ_{Cu}=4/9. We cannot conclude, based on these SEXAFS data only, whether in this case there is a similar registry between the UPD layer and the platinum surface. The appearance of such an open phase might also indicate the possibility that the electrodeposited copper is partially charged. This is a point we had already made in discussing the XANES spectra for submonolayer coverages, and the SEXAFS results here appear to be consistent with that. Interestingly, AFM studies of copper UPD on a Au(111) electrode [6a,b] have shown that in sulfate electrolyte, a $(\sqrt{3}x\sqrt{3})R30°$ copper lattice (Γ_{Cu}=1/3) with a Cu-Cu distance of 4.9 Å forms at +0.10V. This open lattice was not observed if perchlorate was used as the supporting electrolyte [6b]. Thus, the authors concluded that this open structure was stabilized by co-adsorption and partial charge transfer. It is quite

likely that the presence of the strongly adsorbed iodine layer plays a similar stabilizing role in our case.

What is perhaps more surprising is the presence of a close-packed phase as well. In this respect, White and Abruña [25] found that for a copper coverage equivalent to 0.3 ML, in the presence of an iodine ad-layer, the Cu-Cu bond distance was 2.88 Å. Although this distance is considerably larger than that for bulk copper, the structure formed still represents a densely packed phase, especially since the nominal coverage was only 0.3 ML. The in-plane Cu-I bond distance of 1.63±0.05 Å is close to that measured for deposition at +0.10V. This is consistent with a picture in which the only iodine backscattering at this distance is the one riding the close-packed copper phase. Furthermore, since only a fraction of the initial electrodeposited copper is in this high-density phase, it is reasonable that we observe a large drop in the intensity of the peak at 1.48 Å in the radial distribution function (Figure 13b) when compared to the full coverage case (Figure 13c). It is possible that the remaining iodine is co-adsorbed on the platinum surface at the open spaces of the low-density copper phase (Figure 11B). This scenario would produce an in-plane projected Cu-I bond length of 3.64 Å, for which we do not observe a peak in the radial distribution function (Figure 13b). Thus we can only speculate that this is a possible arrangement.

To summarize, at +0.20V (half-monolayer coverage) two coexisting phases are observed: a close-packed phase with a Cu-Cu distance of 2.56±0.05 Å and a considerably more open phase with a Cu-Cu bond length of 4.21±0.05 Å. The in-plane projected Cu-I bond length was found to be 1.63±0.05 Å, which suggests that the only

iodine backscattering in the system is the fraction "riding" the close-packed copper phase.

Conclusions

Employing surface EXAFS and its polarization dependence we have been able to characterize the potential and coverage dependent structural changes of copper underpotentially deposited on an iodine treated platinum surface. We find that at a copper surface coverage of half a monolayer (at +0.20V) there are two in-plane Cu-Cu distances: 2.56±0.05 Å and 4.21±0.05 Å. This suggests a coexistence of a close-packed phase with a more open phase. At +0.10V, where the coverage is one monolayer, the Cu-Cu distance dramatically decreases to 2.54±0.05 Å indicative of a close-packed structure. By carrying out polarization dependence studies, we have determined that at full monolayer coverage (+0.10V) the copper UPD layer is incommensurate, over small length scales, with respect to the platinum surface. The iodine ad-layer rides the electrodeposited copper forming a 3x3 unit cell. This interfacial structure is not altered by removal of the bulk copper species in solution after rinsing of the electrode with pure supporting electrolyte. This points out the "stabilizing" effect of the iodine ad-layer, since electrodeposited copper at a bare platinum surface desorbs completely upon rinsing. We are currently carrying out similar studies in the presence of other adsorbates with emphasis on the halides.

Acknowledgments

This work was supported by the Office of Naval Research and the Army Research Office. DA acknowledges support by a MARC Fellowship from the National Institutes of Health, JFR is a Ford Foundation Fellow. CHESS is supported by the National Science Foundation.

Literature Cited

1 a. Kolb, D.M., in H. Gerisher and C. Tobias, eds., Advances in Electrochemistry and Electrochemical Enginneering, **1978**, Vol. 11, J. Wiley and Sons, New York.

b. Adzic, R. Isr. J. Chem. **1979** 18, 166

c. Adzic, R., in H. Gerisher and C. Tobias, eds., Advances in Electrochemistry and Electrochemical Enginneering,**1985**, Vol. 13, J. Wiley and Sons, New York.

d. Juttner, K.; Lorenz, W.J.; Zeit. Physik. Chemie, **1980**, 122, 163

e. Lorenz, W.J.; Hermann, H.D.; Wuthrich, N.; Hilbert, F.; J. Electrochem. Soc., **1974**, 121, 1167

2 a. Schultze, J.W.; Dickertmann, D. Symp. Faraday Soc. **1977**, 12, 36

b. Salvarezza, R.C.; Vasquez Moll, D.V.; Giordano, M.C.; Arvia, A.J. J. Electroanal. Chem. **1986**, 213, 301

c. Parajon Costa, B.; Canullo, J; Vasquez Moll, D.V.; Salvarezza, R.C.; Giordano, M.C.; Arvia, A.J. J.Electroanal. Chem. **1988**, 244, 261

3 a. Schultze, J.W.; Dickertmann, D. Surf. Sci. **1976**, 54, 489

b. Bewick, A.; Thomas, B. J. Electroanal. Chem.**1976**, 70, 239

4 a. Hubbard, A.T.; Accts. Chem. Res., **1980**, 13, 987

b. Yeager, E.B.; J. Electroanal. Chem., **1981**, 128, 1600

c. Ross, P.N.; Surf. Sci., **1981**, 102, 463

d. Kolb, D.M.; Zeit. Physik. Chemie N.F., **1987**, 154, 179

e. Hubbard, A.T.; Chem. Rev., **1988**, 88, 633

f. Beckmann, H.O.; Gerisher, H.; Kolb, D.M.; Lehnpfuhl, G. Symp. Faraday Soc.**1977**, 12, 51

g. Paffett, M. T.; Campbell, C. T.; Taylor, T. N.; Langmuir, **1985**, 1, 741

h. Leung, L. W. H.; Gregg, T.s W.; Goodman, D. W.; Chem. Phys. Lett., **1992**,188, 467

i. Stuve, E. M.; Rogers, J. W., Jr.; Ingersoll, D.; Goodman, D. W.; Thomas, M. L.; Paffett, M. T.; Chem. Phys. Lett., **1988**, 149, 557

5 a. Stickney, J.L.; Rosasco, S.D.; Song, D.; Soriaga, M.P.; Hubbard, A.T. Surf. Sci. **1983**, 130, 326

b. Hubbard, A.T.; Stickney, J.L.; Rosasco, S.D.; Soriaga, M.P.; Song, D. J. Electroanal. Chem. **1983**, 150, 165

c. Stickney, J.L.; Rosasco, S.D.; Hubbard, A.T. J. Electrochem. Soc. **1984**, 131, 260

6. a. Magnussen, O.M.; Hotlos, J; Nichols, R.J.; Kold, D.M.; Behm, R.J. Phys Rev Lett. **1990**, 64, 2929

b. Manne, S.; Hansma, P.K.; Massie, J.; Elings, V.B.; Gewirth, A.A. Science, **1991**, 251,183

c. Hachiya, T.; Honbo, H.; Itaya, K.; J. Electroanal. Chem. **1991**, 315, 275

7 Abruña, H. D. ed. "Electrochemical Interfaces: Modern Techniques for In-Sitiu Interface Characterization" VCH, New York, N.Y. 1991

8 a. Abruña, H.D.; White, J.H.; Albarelli, M.J.; Bommarito, G.M.; Bedzyk, M.J.; McMillan, M.J. J. Phys. Chem. **1988**, 92, 7045

b. Tourillon, G.; Guay, D.; Tadjeddine, A. J. Electroanal. Chem. **1990**, 289, 263

c. Tadjeddine, A. J.; Guay, D.; Ladouceur, M.; Tourillon, G. Phys. Rev. Lett. **1991**, 66, 2235

d. Samant, M. G.; Borges, G. L.; Gordon, J. G.; Melroy, O. R.; Blum, L.; J. Amer. Chem. Soc. **1987**, 109, 5970

9 a. Samant, M.G.; Toney, M.F.; Borges, G.L.; Blum, L.; Melroy, O.R. J. Phys. Chem. **1988**, 92, 220

b. Toney, M.F.; Gordon, J.G.; Samant, M G.; Borges, G.L.; Wiesler, D.G.; Yee, D.; Sorensen, L.B. Langmuir, **1991**, 7, 796

c. Toney, M. F.; Gordon, J. G.; Samant, M. G.; Borges, G. L.; Melroy, O. R.; Yee, D.; Sorensen, L. B.; Phys. Rev. B: Condens. Matter, **1992**, 45, 9362

10. Bedzyk, M.J.; Bommarito, G.M.; Caffrey, M.; Penner, T. Science, **1990**, 52, 248

11 a. Bommarito, G.M.; White, J.H.; Abruña, H.D. J. Phys. Chem. **1990**, 94, 8280

b. Abruña, H. D.; Bommariro, G. M; Acevedo, D.; Science, **1990**, 250, 69

12 a. Sayers, D.E.; Stern, E.A.; Lytle, F.W.; Phys. Rev. Lett., **1971**, 27, 1204.

b. Stern, E.A.; Phys. Rev. B, **1974**, 10, 3027.

c. Stern, E.A.; Sayers, D.E.; Lytle, F.W.; Phys. Rev. B, **1975**, 11, 4836

For reviews see:

d. Stern, E.A.; Sci. Am., **1976**, 234, 96.

e. Eisenberger, P.; Kincaid, B.M.; Science **1978**,, 200, 1441.

f. Cramer, S.P.; Hodgson, K.O.; Prog. Inorg. Chem., **1979** 25, 1.

g. Teo, B.K.; Accts. Chem. Res.,**1980**, 13, 412.

h. Lee, P.A.; Citrin, P.H.; Eisenberger, P.; Kincaid, B.M.; Rev. Mod. Phys., **1981**, 53, 769

i. Teo, B.K.; Joy, D.C. eds.; "EXAFS Spectroscopy; Techniques and Applications," Plenum, New York, 1981.

j. Teo, B.K.; "EXAFS: Basic Principles and Data Analysis," Springer Verlag, Berlin, 1986.

13 a. Teo, B.K.; Lee, P.; J. Am. Chem. Soc. **1979**, 101, 2815

b. McKale, A.G.; Veal, B.W.; Paulikas, A.P.; Chan S-K.; Knapp, G.S.; J. Am. Chem. Soc. **1988**, 110, 3763

14. Citrin, P.H.; Eisenberger, P.; Kincaid, B.M.; Phys. Rev. Lett. **1976**, 36, 1346.

15. Citrin, P.H.; Journal de Physique; Colloque, C8, **1986**, 47, 437.

16. Stohr, J.; Jaeger, R.; Brennan, S.; Surf. Sci. **1982**, 117, 503

17. Conway, B. E.; Angerstein-Kozlowska, H.; Sharp, W. B. A.; Anal. Chem. **1973**, 45, 1331

18. Bommarito, G. M.; Acevedo, D,; Rodríguez, J. F.; Abruña, H. D. (manuscript in preparation)

19. Aberdam, D.; Durand, R,; Faure, R,; El-Omar, F. Surf. Sci. **1986**, 171, 303

20. White, J.H.; Abruña, H.D. J. Phys. Chem. **1988**, 92, 7131.

21. Lu, F.; Salaita, G.N.; Baltruschat, H.; Hubbard, A.T.; J. Electroanal. Chem. **1987**, 222, 305.

22. Bedzyk, M. J.; Bilderback, D. H.; White, J. H.; Bommarito, G. M.; Abruña, H. D.; J. Phys. Chem. **1986**, 90, 4926

23. Felter, T. E.; Hubbard, A. T.; J. Electroanal. Chem. **1979**, 100, 473

24. Yee, H. S.; Abruña, H. D., Langmuir (in press)

25. White, J. H.; Abruña, H. D.; J. Electroanal. Chem. **1989**, 274, 185

Figure Legends

Figure 1 Comparison of the phase shift determined from ab-initio calculations [13] (lines) and measured from reference materials (symbols) for Cu-Cu (open triangles), Cu-I (filled triangles), and Cu-Pt (filled circles) absorber-backscatterer pairs.

Figure 2 (A) The cyclic voltammetry of a clean platinum/carbon LSM in 0.10M H_2SO_4 electrolyte at a scan rate of 10 mV/sec. Note that in the hydrogen adsorption region (+0.05V to -0.20V) only one pronounced wave is visible, the one corresponding to weak hydrogen adsorption. This voltammetry is in good agreement with that of a Pt(111) electrode which, after flame annealing, was cycled through a series of oxidation-reduction cycles between +1.20V and -0.20V, as shown in (B). Also shown in (A), is the voltammetry after adsorption of an iodine layer (dashed line) in sulfuric acid supporting electrolyte. The iodine covered platinum surface is passivated as illustrated by the absence of the hydrogen adsorption waves. The series of voltammograms in (B) start with the one showing the "butterfly" features at +0.10V, characteristic of a clean, well-ordered over long range Pt(111) surface and shows the progressive transformation to a final steady-state cyclic voltammogram characteristic of a randomly stepped

Pt(111) surface [19] and almost identical to the LSM case depicted in (A). Voltammograms in (B) are also for 0.10M H_2SO_4 and a 10mV/sec scan rate.

Figure 3 Cyclic voltammogram of the UPD of copper on an iodine covered platinum surface of a Pt/C LSM (A) and (B) same as (A) but for a Pt(111) surface which has been reduced-oxidized through a series of cycles prior to iodine adsorption. All voltammetry is in 0.10M H_2SO_4 at a scan rate of 1mV/sec.

Figure 4. (a) Copper coverage isotherms for rinsing and no rinsing experiments derived from electrochemical measurements. (b) same as (a) but for isotherms derived from x-ray fluorescence measurements. (c) the fractional coverage loss due to rinsing of the electrode surface with pure electrolyte, for both electrochemical and x-ray data.

Figure 5. X-ray and electrochemical derived isotherms plotted on an absolute coverage scale after the two data sets were normalized at one point: +0.10V after rinsing.

Figure 6. XANES spectra for copper underpotential deposition at +0.10V, without rinsing. The XANES corresponding to several reference materials (Cu foil, CuI, CuO, $CuPt_3$ and $CuSO_4$) are also shown.

Figure 7. The potential dependence of the XANES for copper deposited at +0.10V, +0.20V, +0.25V, and +0.45V without rinsing, corresponding to nominal coverages of 1, 1/2, 1/4 and 0 monolayers. The vertical offsets are real and represent changes in the coverage. Note that at +0.45V the XANES data shows a prominent "white-line" feature characteristic of copper in a +2 oxidation state (see text). In addition we show the XANES for deposition at +0.10V after rinsing.

Figure 8. Fluorescence detected SEXAFS spectra for copper deposited at +0.10V on an iodine pre-treated platinum surface after rinsing with pure supporting electrolyte, and when the plane of polarization of the x-ray beam was normal to (A) or in the plane (B) of the electrode surface.

Figure 9. (A) Radial distribution function for copper deposited at +0.10 V on an iodine pre-treated platinum surface after rinsing, when the polarization of the x-ray beam was normal to the electrode surface.

(B) EXAFS vs. wavevector for raw and Fourier filtered data as well as the best fit for copper deposited at +0.10 V on an iodine pre-treated platinum surface after rinsing, when the polarization of the x-ray beam was normal to the electrode surface.

Figure 10. (A) Radial distribution function for copper deposited at +0.10 V on an iodine pre-treated platinum surface after rinsing, when the polarization of the x-ray beam was perpendicular to the plane of the electrode surface.
(B) EXAFS vs. wavevector for raw and Fourier filtered data as well as the best fit for copper deposited at +0.10 V on an iodine pre-treated platinum surface after rinsing, when the polarization of the x-ray beam was perpendicular to the plane of the electrode surface.

Figure 11. Schematic depiction of the structure of copper deposited on an iodine pre-treated platinum surface for deposition at: +0.10V corresponding to the full coverage case (A), and +0.20V corresponding to a half-monolayer coverage (B). See text for discussion.

Figure 12. Fluorescence detected SEXAFS spectra for copper deposited at +0.10V (A) and +0.20V (B) on an iodine pre-treated platinum surface without rinsing, and when the plane of polarization of the x-ray beam was in the plane of the electrode surface.

Figure 13. Radial distribution function for copper foil (a) and for copper deposited at +0.20 (b) and +0.10 V (c) on an iodine pre-treated platinum surface without rinsing. The polarization of the x-ray beam was in the plane of the electrode surface.

SEXAFS Results for Cu Underpotential Deposition on an I Treated Pt/C LSM

+0.1 V, After Rinsing								+0.1V, No Rinsing				+0.2V, No Rinsing			
σ polarization				π polarization				σ polarization				σ polarization			
Bond Type	R (Å)	N Eff.	DW (Å)	Bond Type	R (Å)	N Eff.	DW (Å)	Bond Type	R (Å)	N Eff.	DW (Å)	Bond Type	R (Å)	N Eff.	DW (Å)
Cu-Cu	2.54	6.4	0.063	Cu-I	3.10	1.0	0.064	Cu-Cu	2.56	5.9	0.067	Cu-Cu	2.56	6.2	0.065
Cu-I	1.52	1.2	0.071	Cu-Pt	2.44	2.1	0.082	Cu-I	1.56	1.9	0.069	Cu-Cu	4.21	5.3	0.084
Cu-Pt	1.41	0.6	0.095					Cu-Pt	1.44	0.5	0.098	Cu-I	1.63	1.3	0.072

All bond lengths (R) are ± 0.05 Å
All effective coordination numbers (N Eff.) are ± 20%
All Debye-Waller (DW) factors are ±0.01 Å

Bond Lengths Determined from SEXAFS Data for Cu UPD at +0.1 V, After Rinsing			
Bond	SEXAFS (Ang.)	Expected (Ang.)	
Cu-Cu	2.54	2.56	Atomic-Atomic
Cu-I	3.45	3.48	Atomic-VdW
Cu-Pt	2.82	2.67	Atomic-Atomic

Calculated In-Plane and Out-of-Plane Bond Length Components for Various Surface Sites			
In-Plane Bond	Surface Site 3-Fold (Ang.)	Bridge (Ang.)	Top (Ang.)
Pt-Cu	1.61	1.39	0.00
Cu-I	1.48	1.28	0.00
Out-of-Plane Bond	Surface Site 3-Fold (Ang.)	Bridge (Ang.)	Top (Ang.)
Pt-Cu	2.13	2.28	2.67
Cu-I	3.15	3.24	3.48

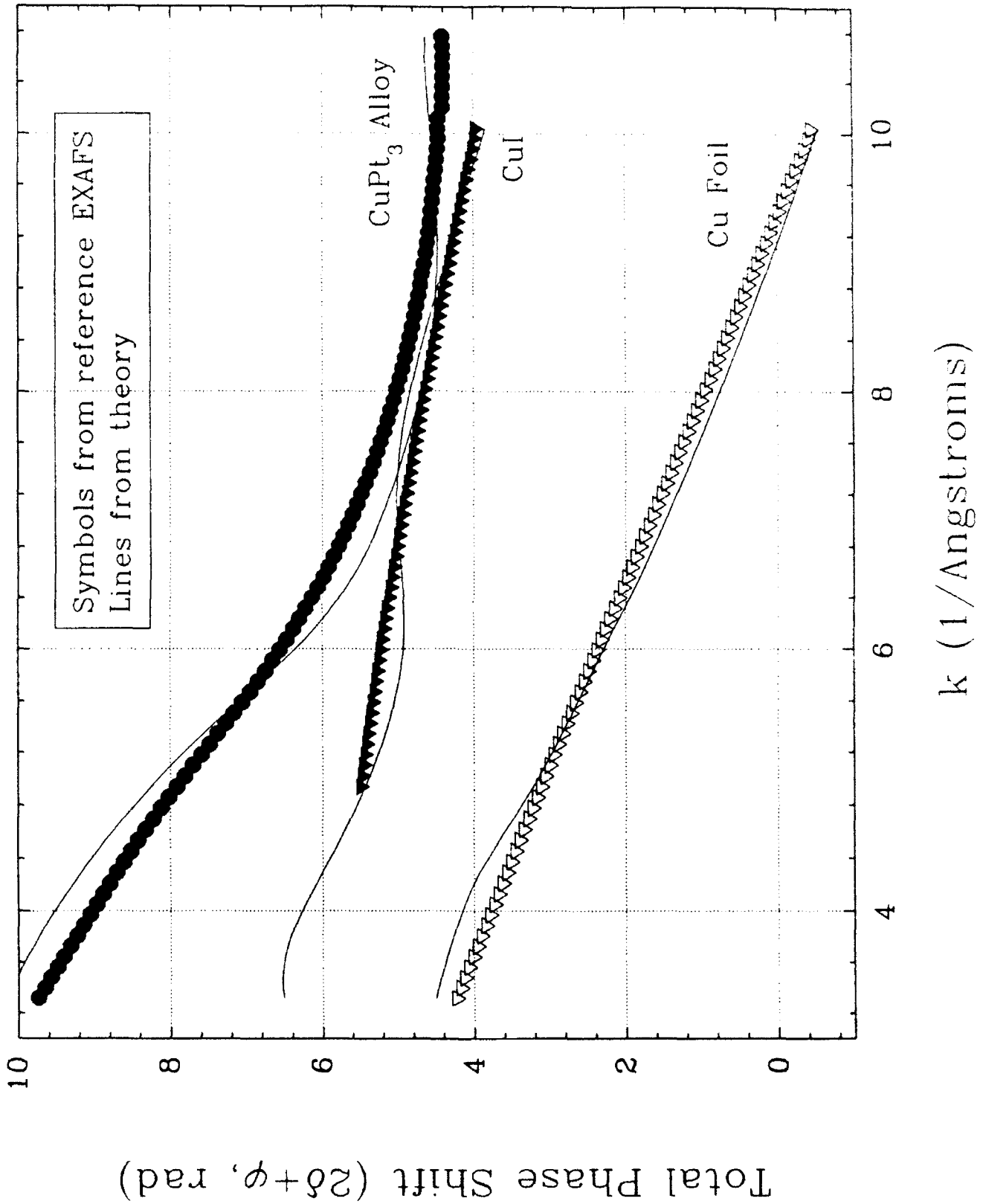
Symbols from reference EXAFS
Lines from theory
$CuPt_3$ Alloy
CuI
Cu Foil
Total Phase Shift (2δ+φ, rad)
k (1/Angstroms)
0
2
4
6
8
10
4
6
8
10

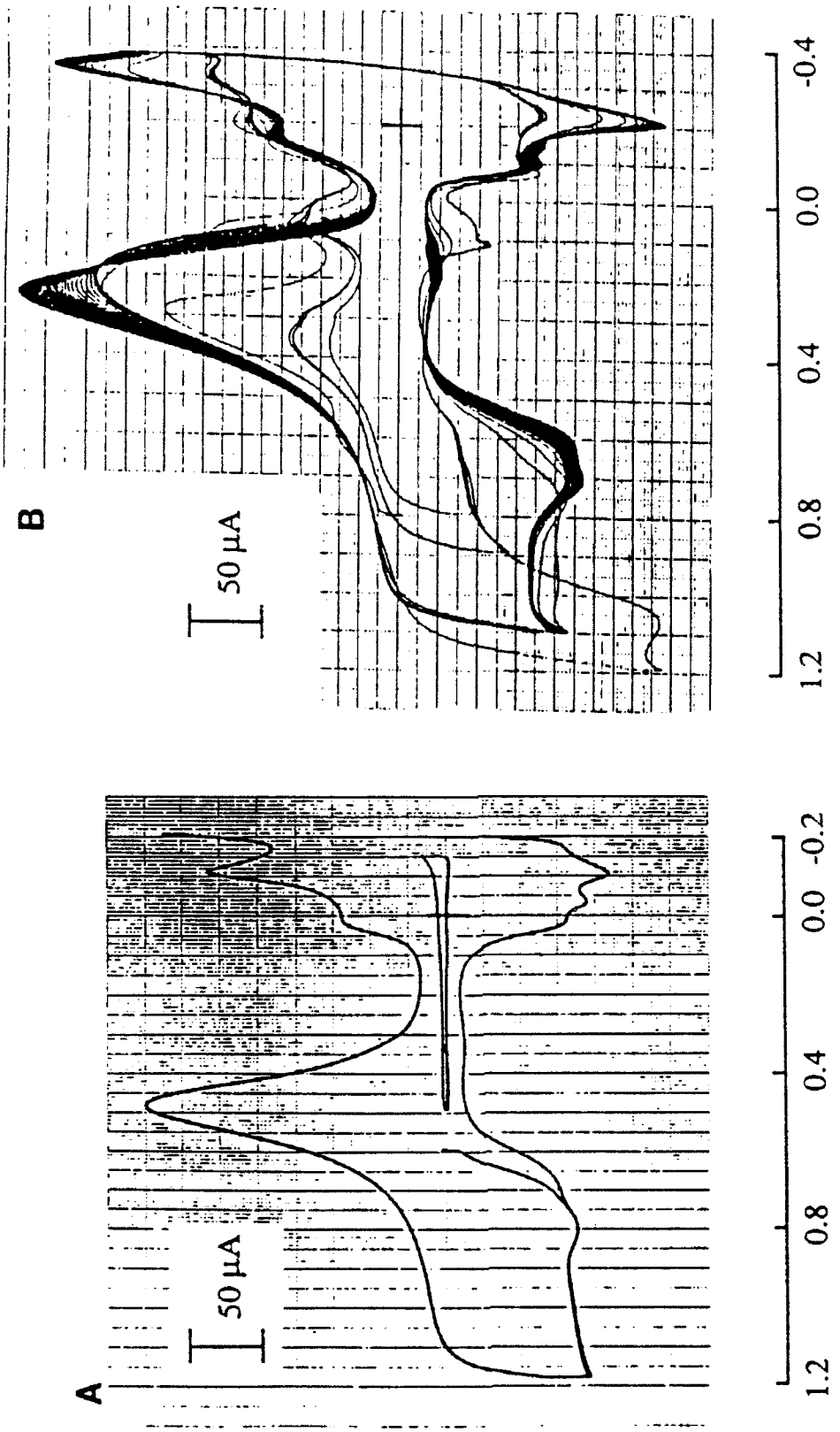
B
50 µA
1.2
0.8
0.4
0.0
-0.4
V vs. Ag/AgCl
A
50 µA
1.2
0.8
0.4
0.0
-0.2
V vs. Ag/AgCl

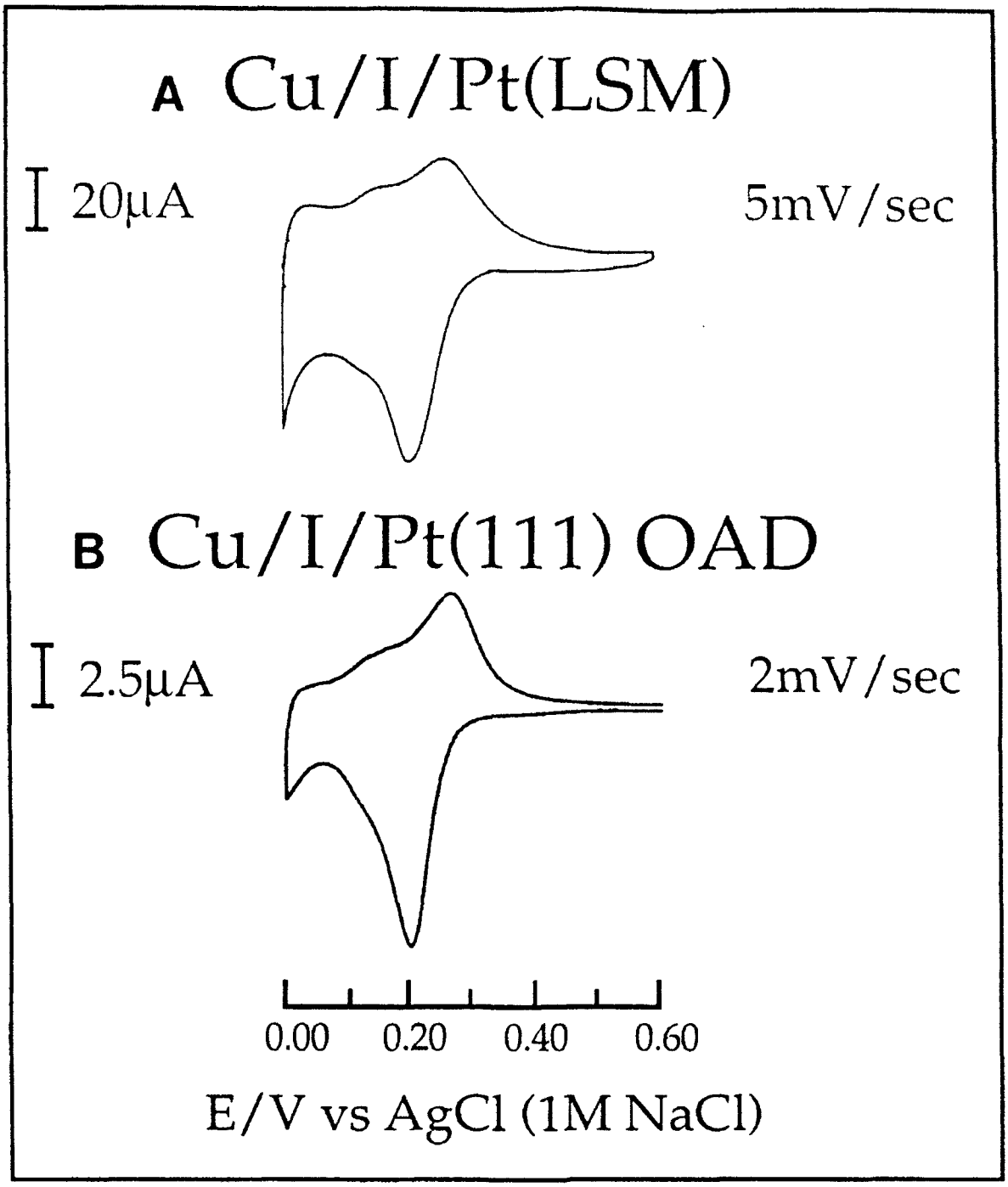
A Cu/I/Pt(LSM)
20μA
5mV/sec
B Cu/I/Pt(111) OAD
2.5μA
2mV/sec
0.00
0.20
0.40
0.60
E/V vs AgCl (1M NaCl)

Bommarito *et al.* / Figure 4

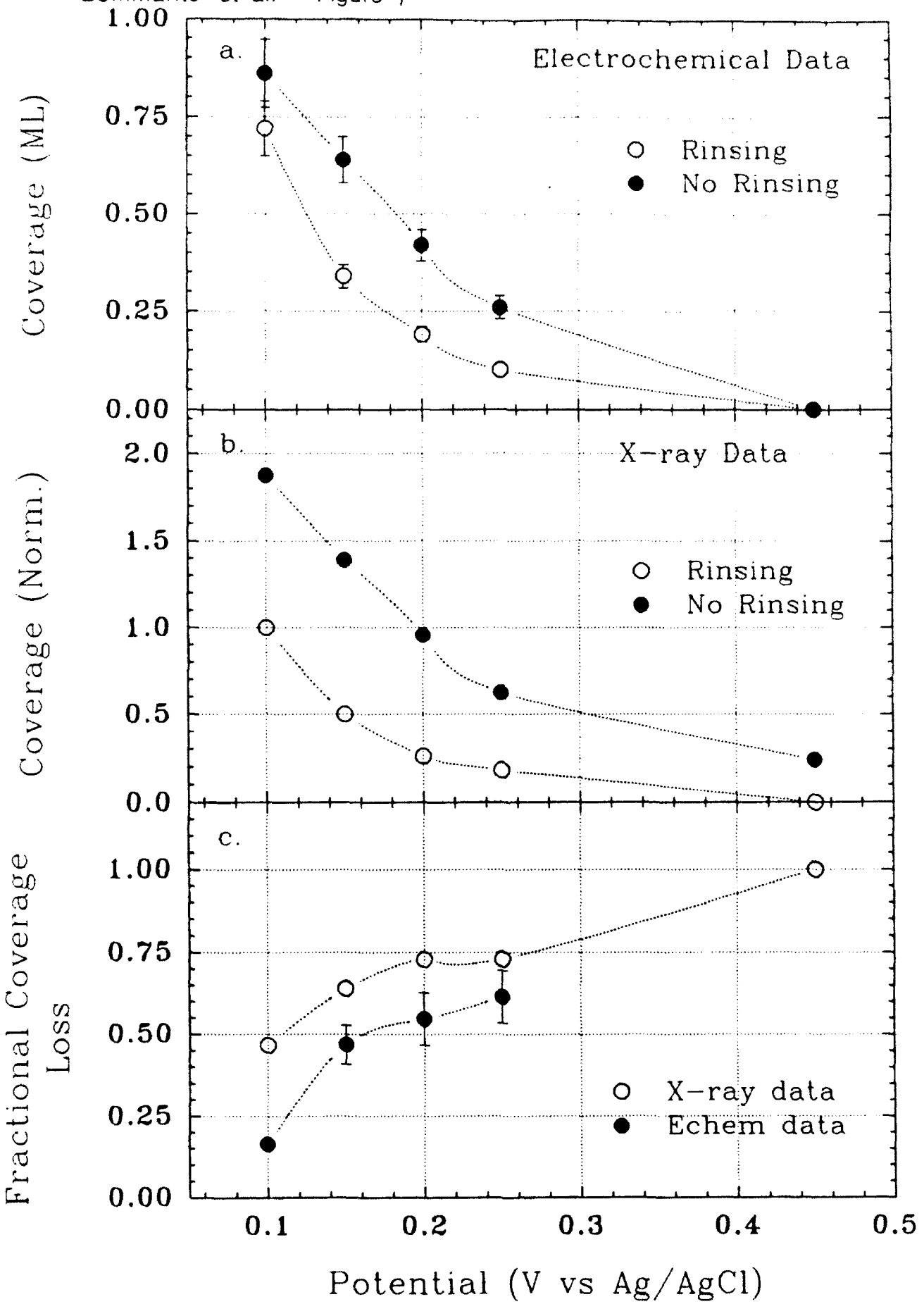

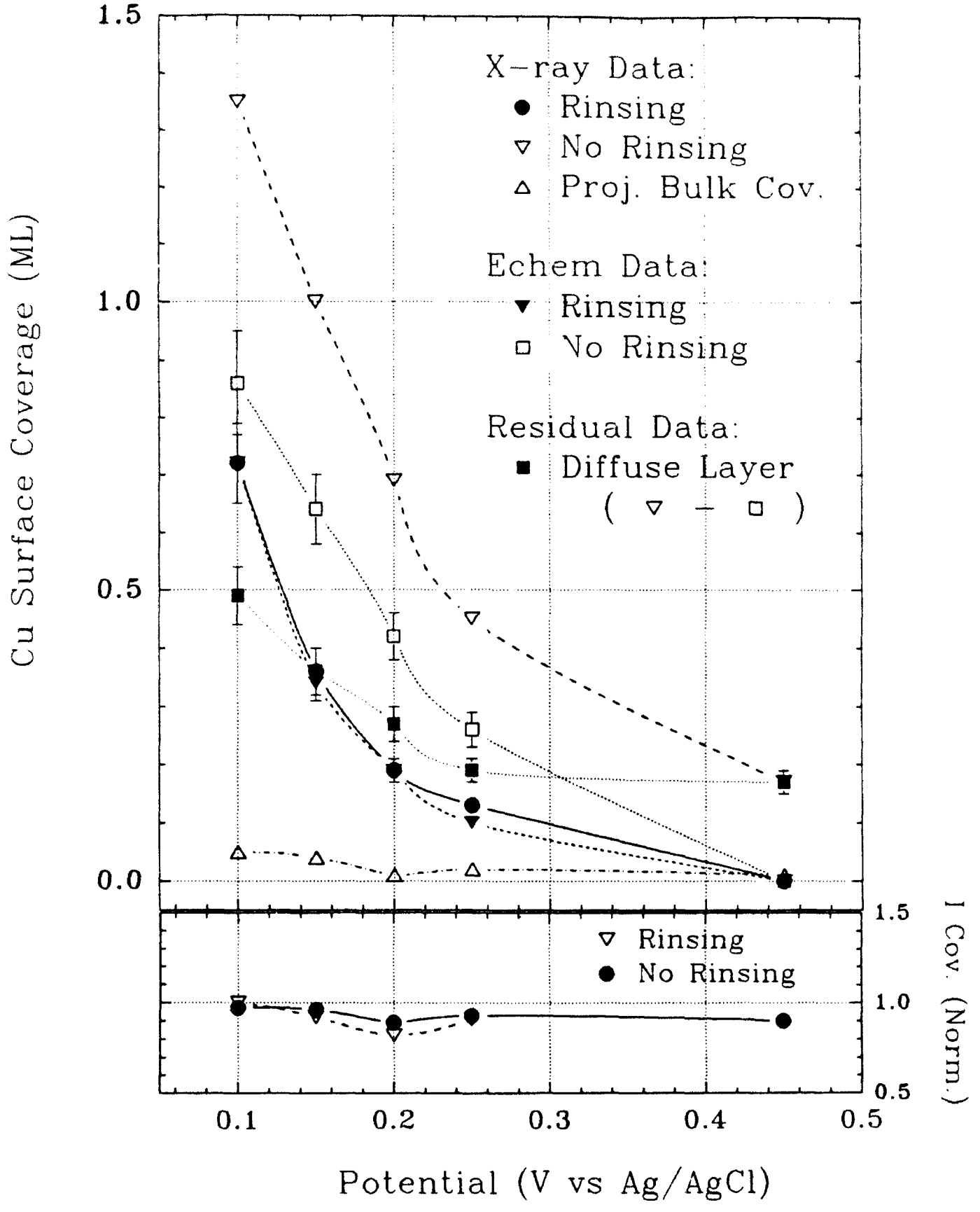
1.5
1.0
0.5
0.0
Cu Surface Coverage (ML)
X-ray Data:
Rinsing
No Rinsing
Proj. Bulk Cov.
Echem Data:
Rinsing
No Rinsing
Residual Data:
Diffuse Layer
(▽ − □)
Rinsing
No Rinsing
1.5
1.0
0.5
I Cov. (Norm.)
0.1
0.2
0.3
0.4
0.5
Potential (V vs Ag/AgCl)

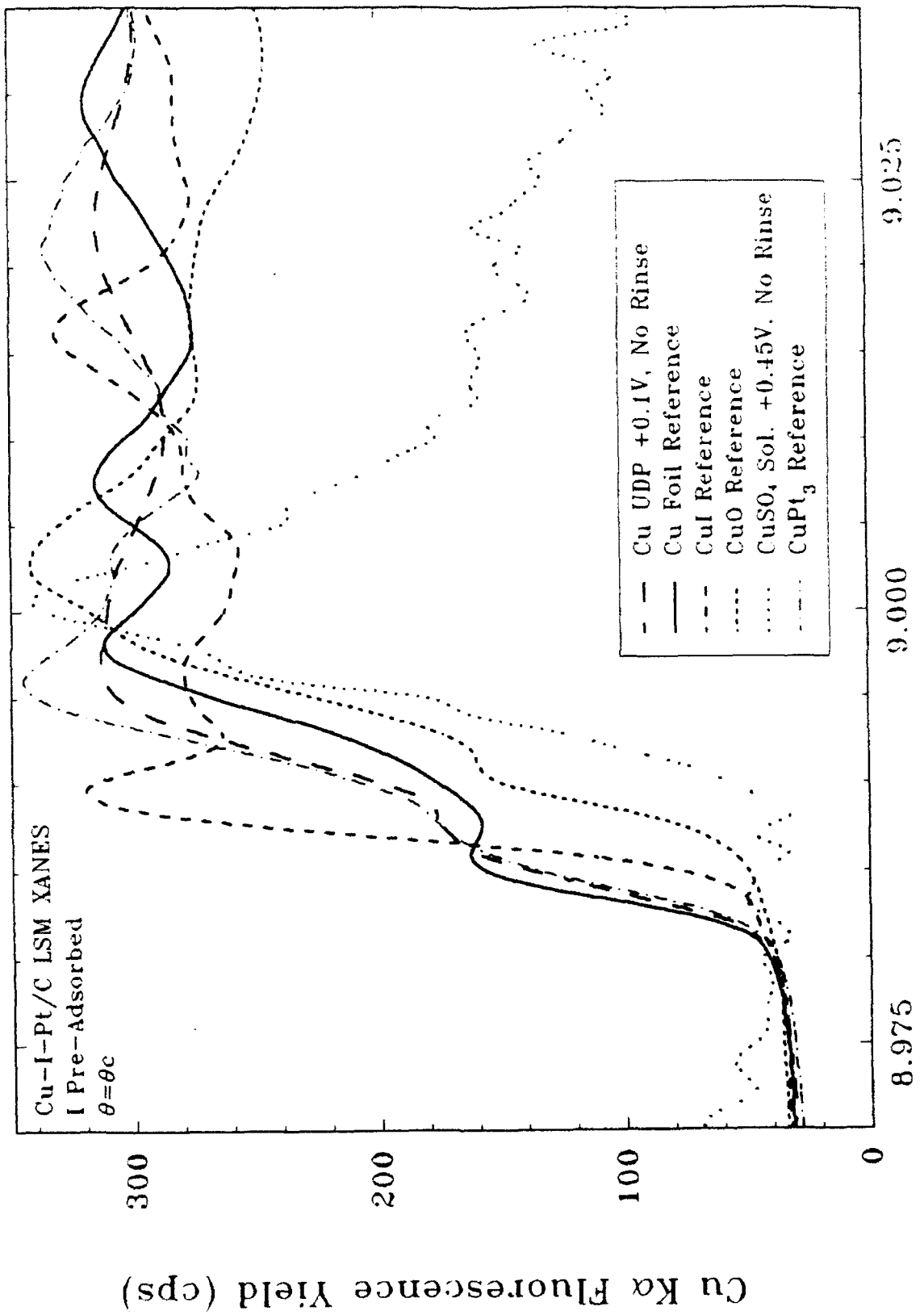
Cu-I-Pt/C LSM XANES
I Pre-Adsorbed
θ=θc
Cu UDP +0.1V, No Rinse
Cu Foil Reference
CuI Reference
CuO Reference
CuSO4, Sol. +0.45V. No Rinse
CuPt3 Reference
Cu Kα Fluorescence Yield (cps)
Energy (keV)
0
100
200
300
8.975
9.000
9.025

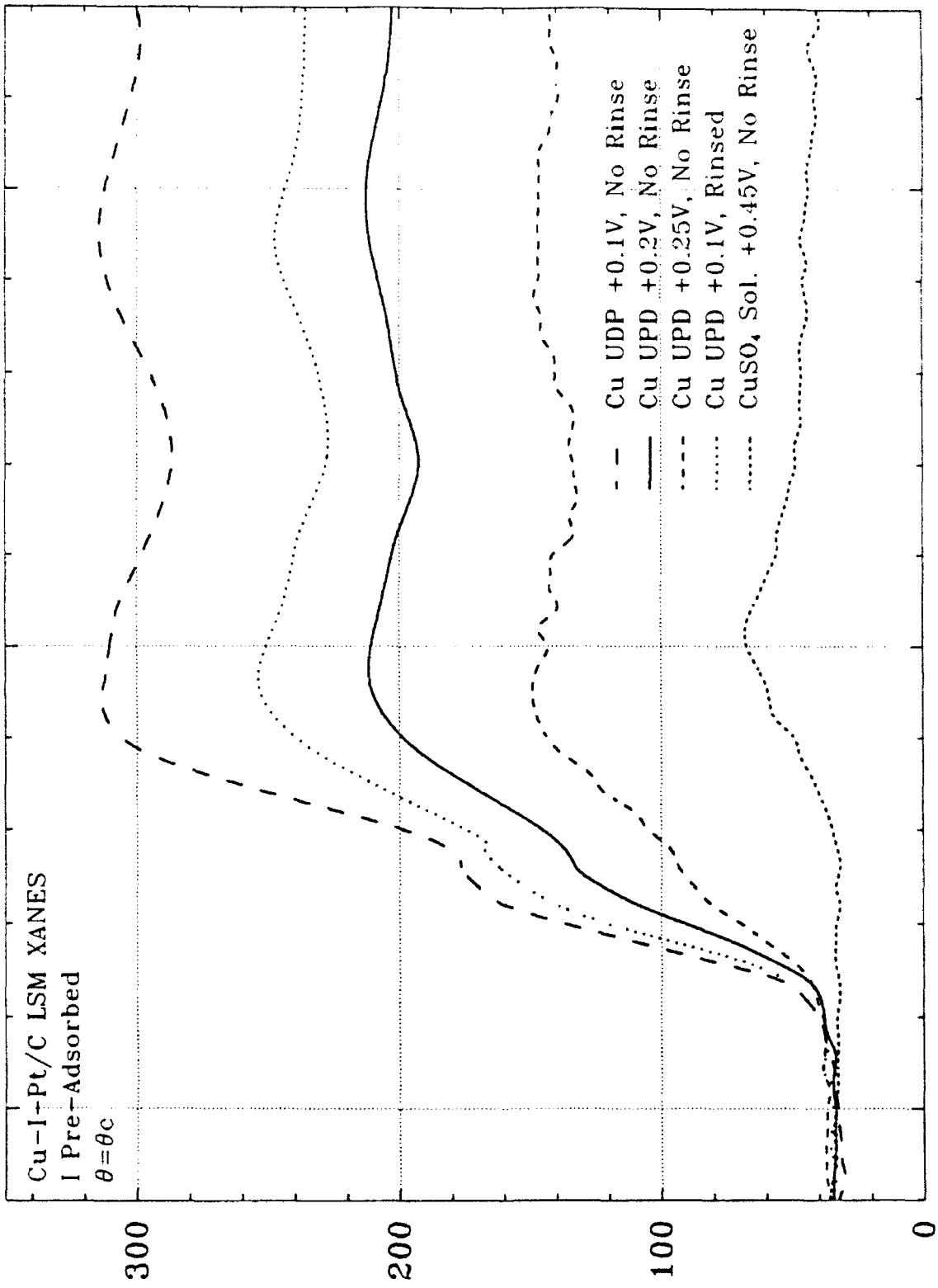
Cu-I-Pt/C LSM XANES
I Pre-Adsorbed
θ=θc
Cu UDP +0.1V, No Rinse
Cu UPD +0.2V, No Rinse
Cu UPD +0.25V, No Rinse
Cu UPD +0.1V, Rinsed
CuSO4 Sol. +0.45V, No Rinse
Cu Kα Fluorescence Yield (cps)
0
100
200
300
8.975
9.000
9.025
Energy (keV)

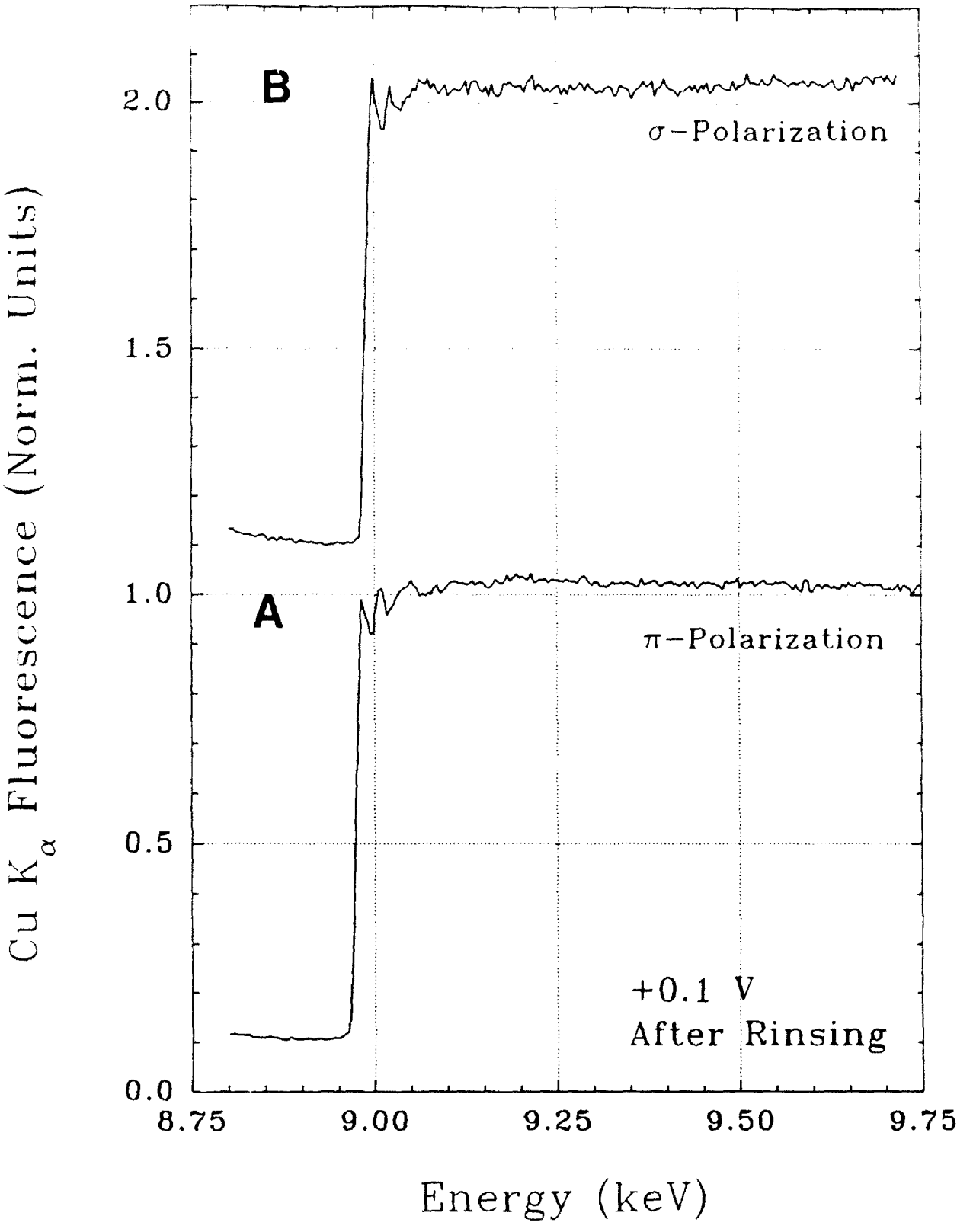
B
σ−Polarization
A
π−Polarization
+0.1 V
After Rinsing
2.0
1.5
1.0
0.5
0.0
8.75
9.00
9.25
9.50
9.75
Cu K_α Fluorescence (Norm. Units)
Energy (keV)

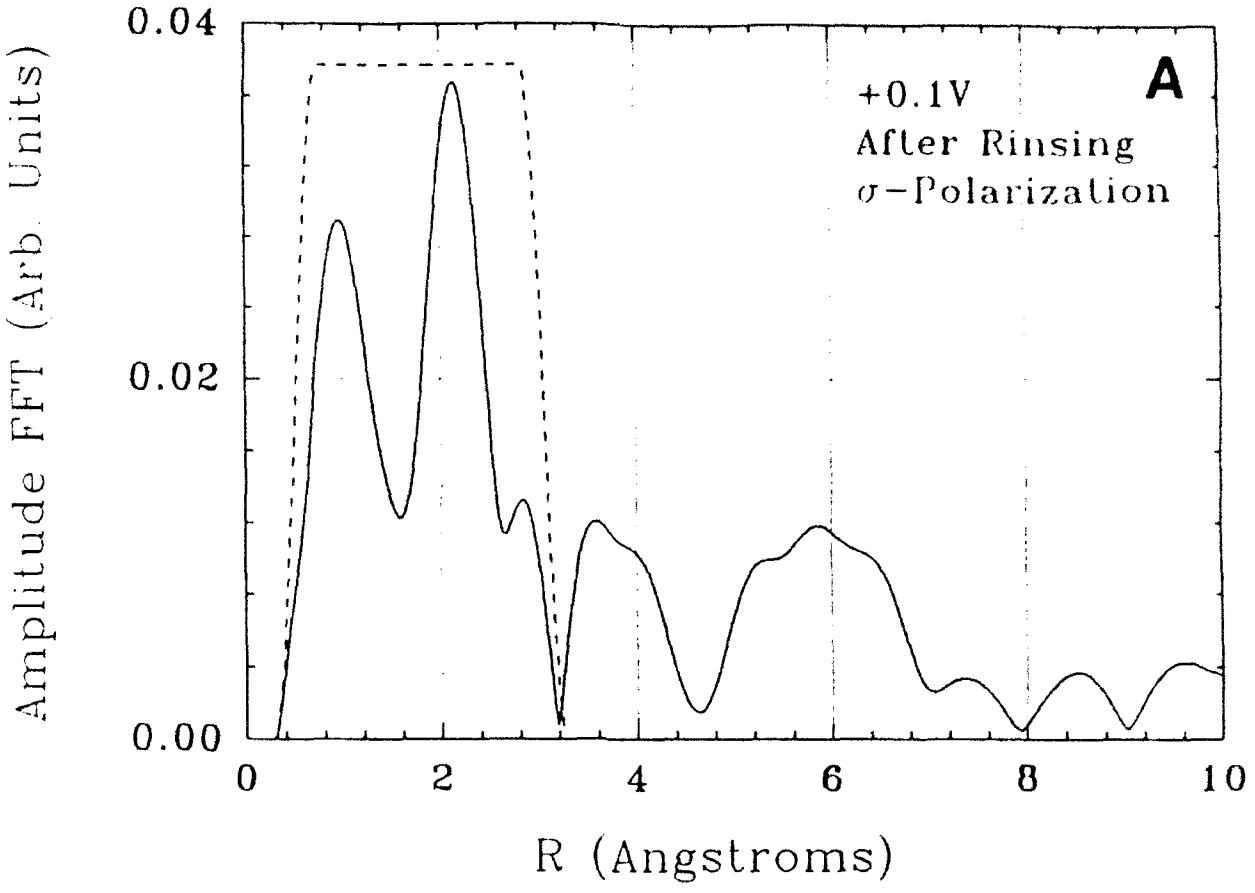
0.04
0.02
0.00
Amplitude FFT (Arb. Units)
+0.1V
After Rinsing
σ−Polarization
A
0
2
4
6
8
10
R (Angstroms)

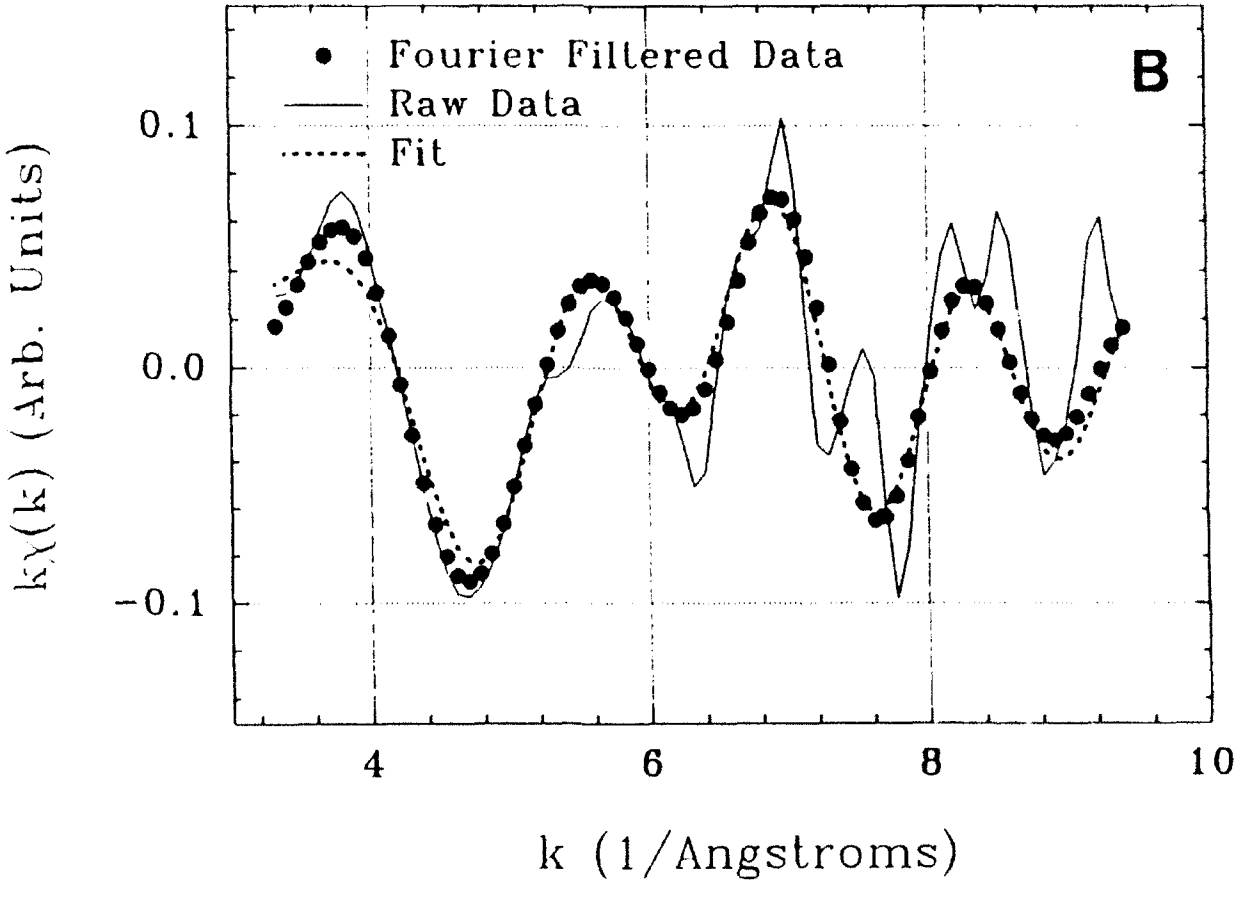
Fourier Filtered Data
Raw Data
Fit
B
0.1
0.0
−0.1
kχ(k) (Arb. Units)
4
6
8
10
k (1/Angstroms)

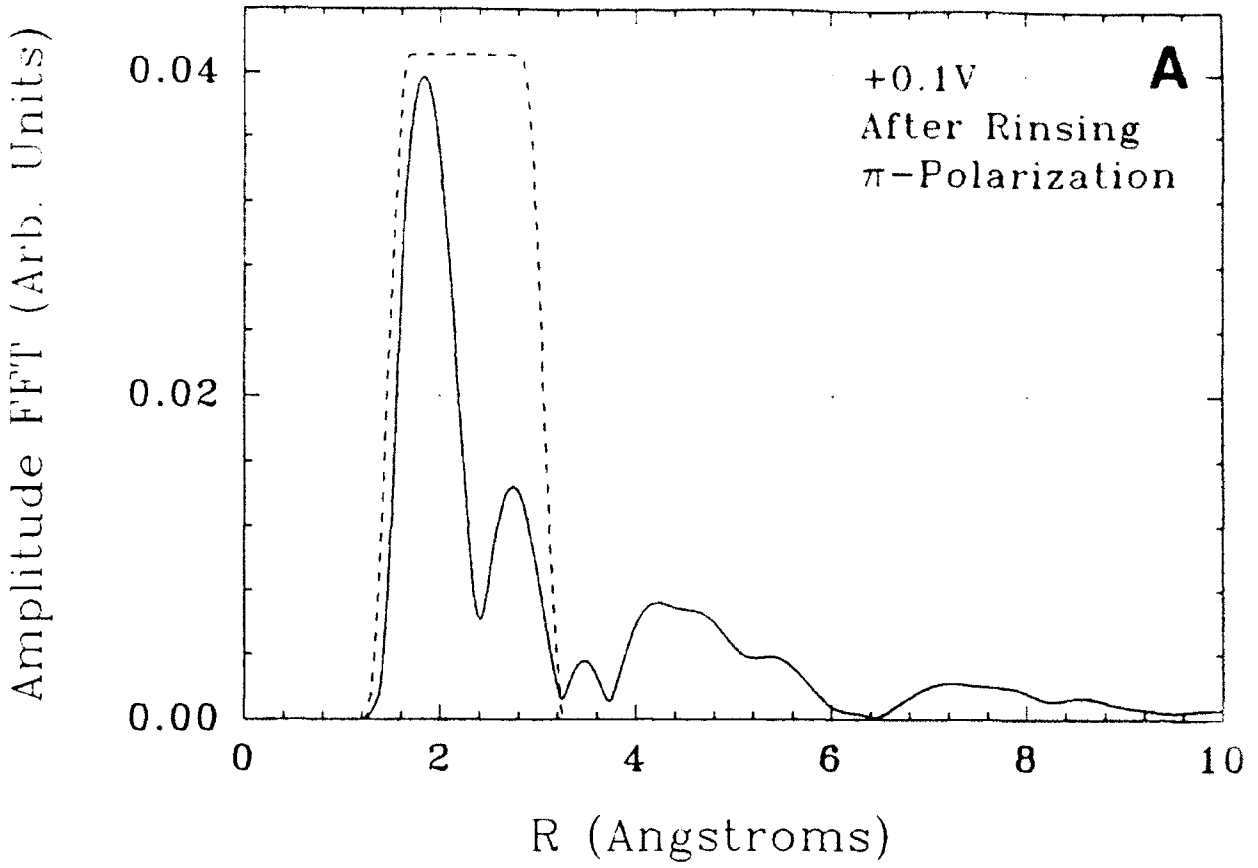
Amplitude FFT (Arb. Units)
0.04
0.02
0.00
0
2
4
6
8
10
R (Angstroms)
+0.1V
After Rinsing
π−Polarization
A

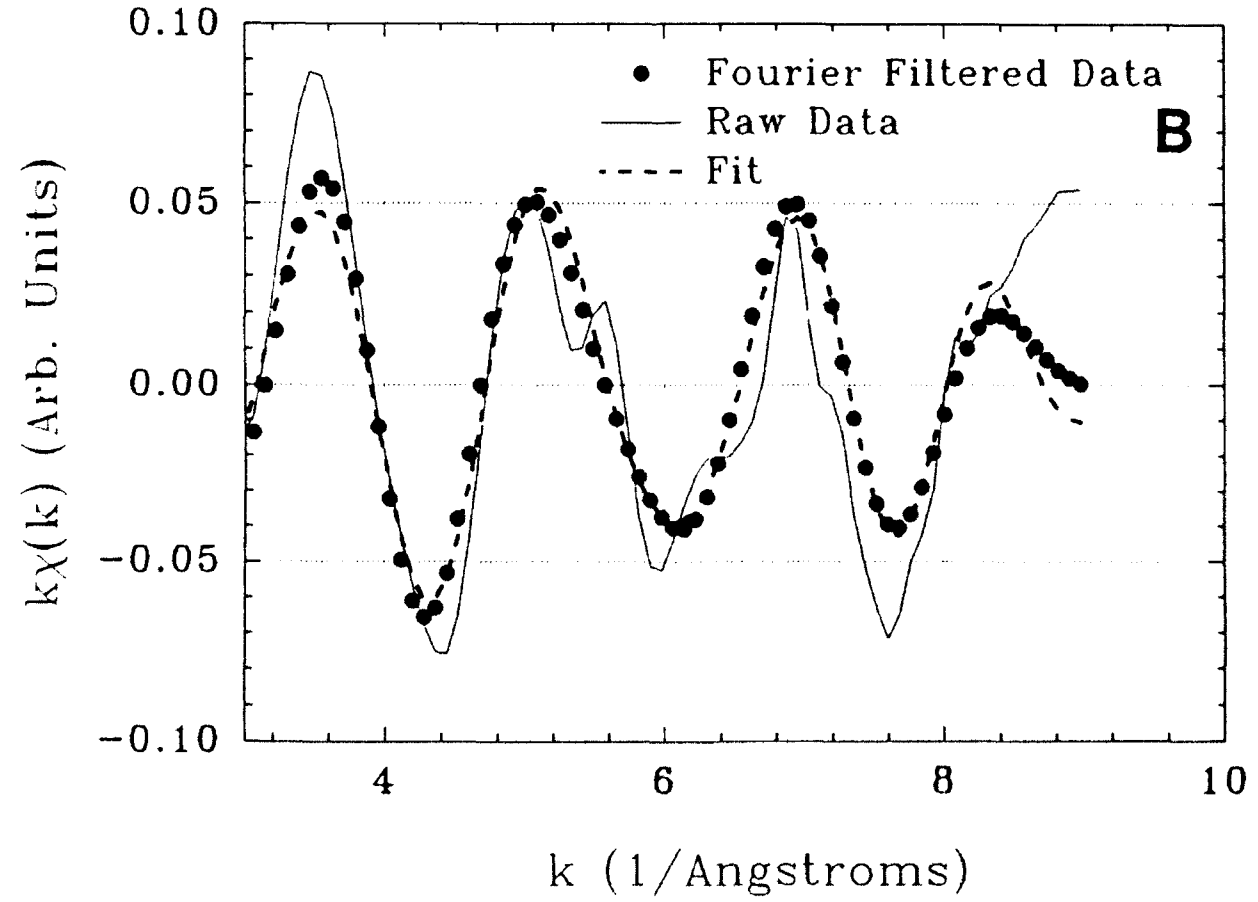
kχ(k) (Arb. Units)
0.10
0.05
0.00
−0.05
−0.10
4
6
8
10
k (1/Angstroms)
Fourier Filtered Data
Raw Data
Fit
B

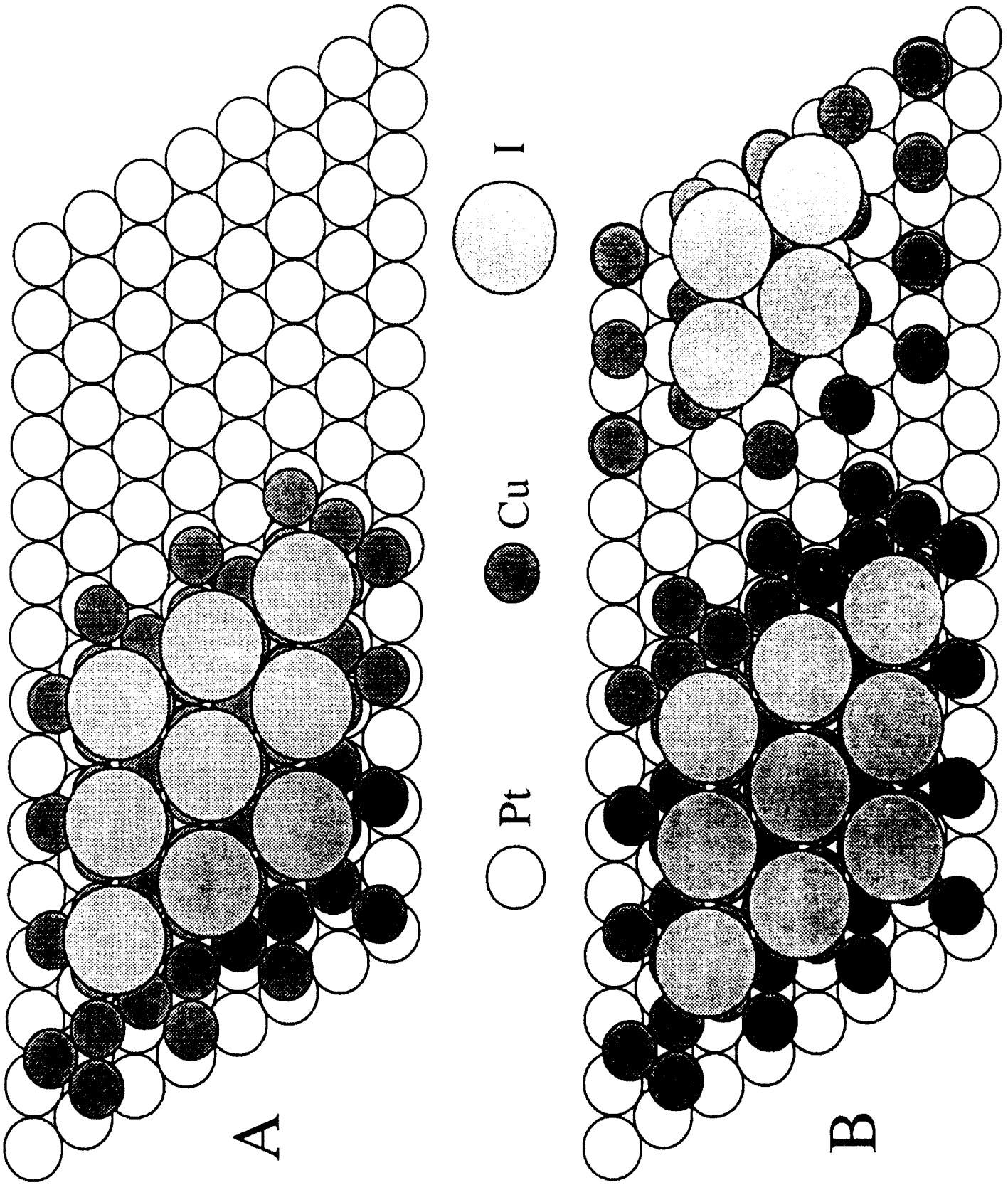
A
I
Cu
Pt
B

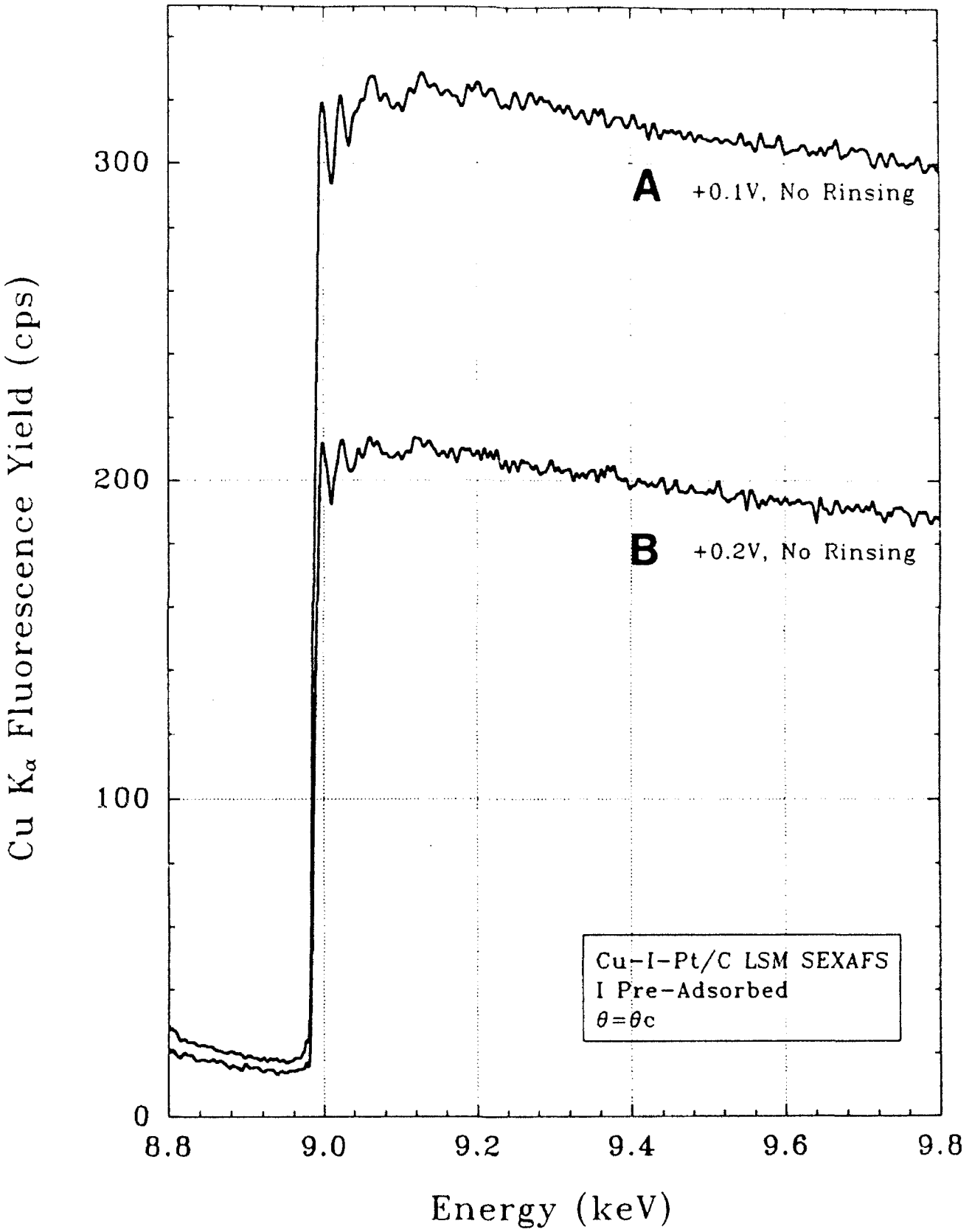
Cu Kα Fluorescence Yield (cps)
300
200
100
0
8.8
9.0
9.2
9.4
9.6
9.8
Energy (keV)
A +0.1V, No Rinsing
B +0.2V, No Rinsing
Cu-I-Pt/C LSM SEXAFS
I Pre-Adsorbed
θ=θc

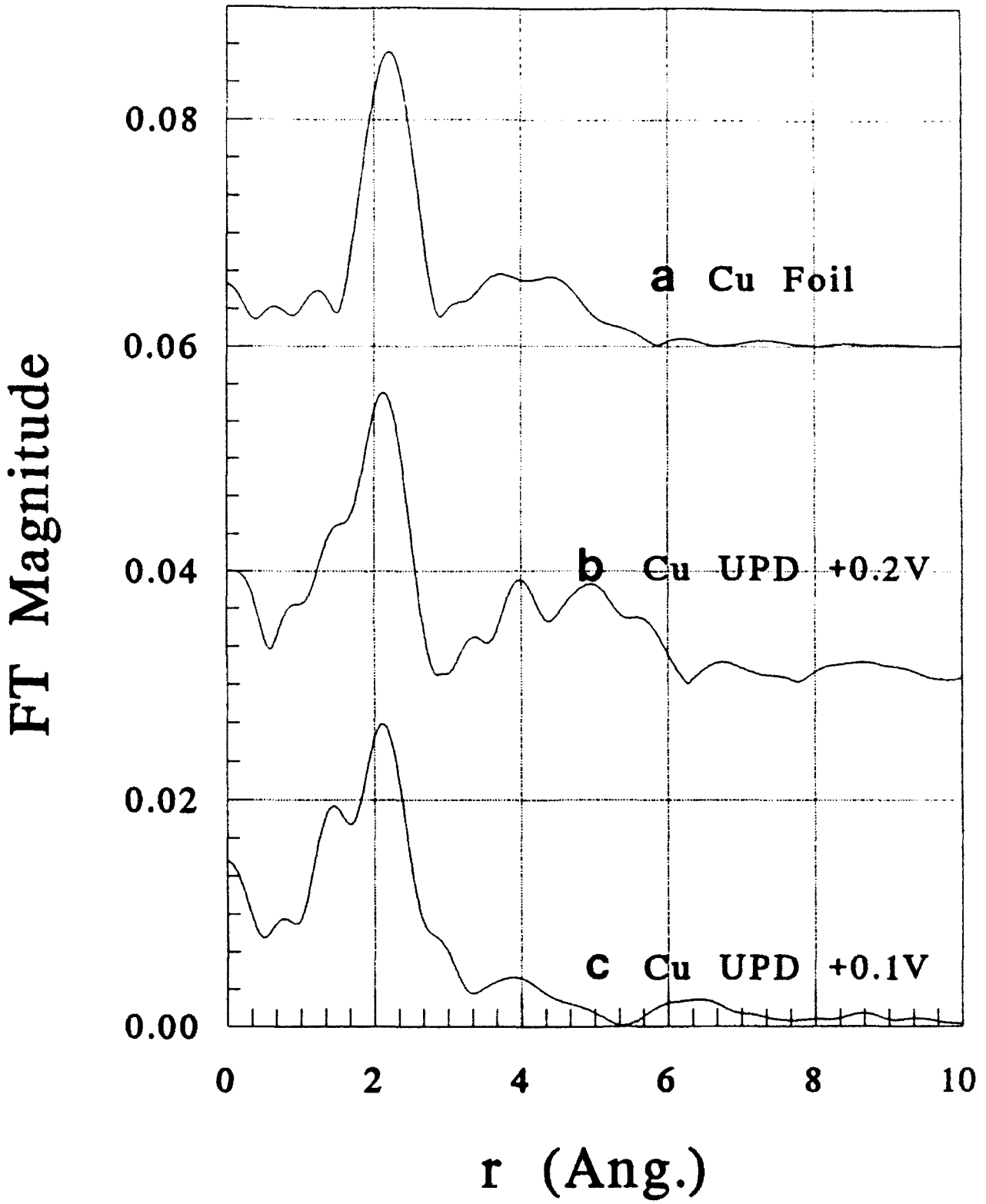
FT Magnitude
0.08
0.06
0.04
0.02
0.00
a Cu Foil
b Cu UPD +0.2V
c Cu UPD +0.1V
0
2
4
6
8
10
r (Ang.)